# Interdisciplinary approaches for 4D Radiotherapy of moving lung tumors based on nonlinear dynamics systems theory

by

**Ranjini P. Tolakanahalli**

A dissertation submitted in partial fulfillment of

the requirements for the degree of

**Doctor of Philosophy**

**(Medical Physics)**

at the

UNIVERSITY OF WISCONSIN - MADISON

2012

**Date of final oral examination:  5/4/2012**

**The dissertation is approved by the following members of the Final Oral Committee:**
    **Tomé, Wolfgang A, Professor, Department of Medical Physics.**
    **Paliwal, Bhudatt R, Professor, Department of Medical Physics**
    **Mackie,  Rockwell , Professor, Department of Medical Physics**
    **Kozak, Kevin R, Assistant Professor, Department of Human Oncology**
    **Ritter, Mark A, Professor, Department of Human Oncology**

# Acknowledgements

Life is a bundle of happiness and tribulations. The human endeavors, however, are to increase the happiness and decrease the sufferings, and at the root of all these is the mind. While spirituality & spiritual therapy remains to be the best holistic approach for all mental ailments, medical intervention becomes important for all bodily ailments and cure. One such ailment that has evaded mankind's conquest of sufferings is Cancer. Thus I sincerely dedicate my hard work as my humble contribution to the conquest over Cancer. '*Work without faith and prayers is like artificial flowers without fragrance*' (from Bhagavad Gita) and '*service to mankind is service to God*' has been my driving force through all times of difficulties, challenges and uncertainties during this work. I thus begin by thanking the almighty God with my work as my sincere offering to him.

I sincerely thank my advisor Prof. Wolfgang Tomé whose unwavering support and timely guidance cleared all hurdles in my path. I also thank Prof. Bhudatt Paliwal for his encouragement, support and accommodation of my work schedules. I express my deepest gratitude to them and will forever remain indebted for all their support and encouragement. I would like to thank all my committee members, Prof. Rockwell Mackie, Prof. Mark Ritter, Prof. Kevin Kozak for their insightful inputs and guidance. I would also like to add special thanks to my colleague, friend and well wisher Dr. Dinesh Tewatia who has helped me countless times in several ways. It was his unwavering support that gave me the confidence to manage both work and research at the same time and I shall forever remain indebted to him for that.

I thank all my colleagues – therapists, dosimetrists, physicians ,resident physicians and all my fellow physicists whose encouragement and support made it humanly possible to cover up

for all the clinical responsibilities. I specially would like to thank Linda Brock and her dog Chloe for being my companions over the last week months. I extend special thanks to Dr. Yadav, Ms. Jialu Yu, Mr. Brad McCabe, Mr. Charles Wallace, Dr. Jennifer Smilowtz, Dr. Adam Bayliss , Mr. Amar Basavatia and Dr. Erich Urban for helping me cover my clinical duties many times during crunch times. Special thanks also to Marcus and Cynthia (Cid) who kept me company on many late evenings, brought me food, always encouraged me and showered me with their kind affection and support.

I offer my heartfelt gratitude to my most beloved husband Mr. Arunkumar Manikundalam, whose unconditional support both physically and mentally, patience, sacrifice and accommodation of my long work hours made it all possible. Without his encouragement and support this would certainly not have been possible.  I want to acknowledge my lifetime inspirations - my dearest father Mr. Prabhakara Tolakanahalli and my dearest mother Mrs. Shylaja T.P. and my loving elder sister Mrs. Nandini Menon. I express my deepest gratitude for all their support throughout my life. I also acknowledge the support and encouragement from my brother-in-law Mr. Praveen Menon. I express my love to my dearest nephew Aniruddh Menon for showing me the joy in pure love. I remain indebted to my in-laws - Mr. M.R. Balasubramanyam and Mrs. Geetha Balasubramanyam for all their love, prayers and good wishes. I thank my sister-in-law Mrs. Ashwini Prashanth and her husband Prashanth for their support.

My acknowledgements would not be complete if I do not extend my thanks to all my friends and well wishers whose influenced me and made me the person I am today. I thus extends my heartful thank Viral Bhatt, Keyur Dani, Vrushali Raut, Richa Gupta, Amit Singh, Cheryan Jacob, Rashmi Parakkal-Bhugra, Ramya Kapadia Nitin Sarwal, Naini Bhatt, Rohan Hathiwala, Nikhil

# Abstract

Nonlinear dynamics based 4D dose guided radiotherapy

for moving tumors

by

Ranjini P. Tolakanahalli

Under the supervision of Professor Wolfgang A. Tomé

Radiation, the mainstay of local nonsurgical treatment for regionally advanced non-resectable non-small cell lung cancer, is associated with poor outcomes due to local failure. Intra-fractional tumor motion mainly due to respiratory motion necessitates enlarged treatment margins to provide full tumor coverage, thus limiting the dose that can be escalated for tumor control. Tumor motion and breathing irregularity are two major hurdles which stop us from achieving this apparently simple goal of dose escalation while sparing normal tissues. Effective compensation to account for this depends on: Firstly, the robustness of the monitoring system for tracking real-time tumor motion and secondly the efficiency of the delivery system in adapting to the observed tumor motion.

Delivery of radiation therapy using synchronization methodologies requires knowledge of real-time tumor position. No matter how robust the methodologies are, they all suffer from the problem of system latency. System latency can be understood as a delay from the instant the tumor moves before the treatment system can make its corrective response. Predicting respiratory motion in real-time is challenging, due to the inherent chaotic nature of breathing patterns, i.e. sensitive dependence on initial conditions. In our previous work we analyzed the breathing pattern of 16 patients using time-delay based state space techniques and established

that respiratory system is 5-6 dimensional nonlinear, stationary and deterministic in nature albeit chaotic with sensitive dependence to initial conditions. In this thesis, we introduce nonlinear prediction algorithms based on state-space methodologies that have a larger prediction horizon than linear methods if an appropriate time delay and embedding dimension are chosen. In addition, a much larger prediction horizon can be achieved if patients can be coached to closely follow a regular breathing pattern. Patients revisit their breathing orbits arbitrarily closely and stay for a while before exponentially diverging from the orbit. These are called Unstable Periodic Orbits (UPOs) which can be used to intelligently coach the patients to maintain a comfortable breathing. This approach is called Chaos Control and its theoretical basis and preliminary results are elucidated in this thesis. However, many patients with high transients can be very challenging for both prediction and chaos control. We also introduce a novel method, Recurrence quantification analysis (RQA) that can be used as a quantitative decision making tool to classify patients breathing pattern. RQA is a promising and powerful tool to decide if a patient is a good candidate for Chaos control and prediction or just prediction bundled with 4D treatment. For highly chaotic breathing patterns, it might be best to adapt with the Maximum Projection Intensity (MIP) Image based Internal Target Volume (ITV) treatments.

# Table of Contents

# List of Figures

# List of Tables

# Chapter 1.  Introduction

Targeting moving tumors for lung cancer tumors during radiation therapy is complicated due to intra-fractional and inter-fractional motion. Advances in Image Guided Radiation Therapy (IGRT) enable one to account for inter-fractional differences thus allowing for margin reduction. Intra-fractional tumor motion which is mainly due to respiratory motion necessitates enlarged treatment margins to provide full tumor coverage. These margins thus limit the dose that can be escalated for tumor control. It is also well accepted that intensity-modulated radiation therapy (IMRT) is known to be more susceptible to tumor motion compared with conventional treatment techniques due to interplay between MLC and tumor motion. Methods to mitigate errors due to motion  include  treating a motion envelope (van Herk, 2004), the average intensity projection of a the motion envelope (Ehler and Tomé, 2008) and modulating the dose rate (Ehler and Tomé, 2009). Changes in the form of the tumor or its position have a significant impact on the actual delivered dose distribution due to steep dose gradients (Bortfeld *et al.*, 2002; Ehler and Tomé, 2008; Ehler *et al.*, 2007).

Gating and synchronization methodologies are two popular methods that are explored vastly in the community.  For synchronization methodologies, the underlying requirement is knowledge of real-time tumor position. Current direct tracking methodologies employ continuous observation of the implanted fiducials in the tumor during treatment using fluoroscopic imaging, but this approach often is not feasible. An underlying requirement of externally monitored surrogate signal to deduce tumor position is spatial and temporal correlation of tumor motion with surrogate signal. Regardless if direct or indirect methods are used for tumor tracking, there always exists a delay before the treatment system can make its corrective response. It has been widely accepted that latency error contributes to a greater dosimetric impact, especially at longer

response times (greater than 200 ms) which demands the need for good prediction algorithms. This delay can range from 50 ms for the beam to be gated to several hundred milliseconds for the beam to be physically realigned. Thus in order to target the tumor in real-time, the position of the tumor must be predicted by the system ahead by a time at least equal to or greater than system latency. Most of the prediction methods are based on autoregressive linear prediction models or sinusoidal-model based predictive filters. Such models have difficulty predicting irregular signals. It has been generally accepted that most prediction algorithms perform better when there is regularity and reproducibility of patient breathing pattern. Most of the linear and non-linear methods mentioned above fail to predict accurately when the system latency is greater than 200 ms with imaging frequency less than 10Hz.

None of the above methods really delve deep into the underlying mechanism governing respiratory breathing. Breathing is a neurophysiological process, which is controlled by the rhythmical centers which are not irregular or random (Rybak et al., 2007). Central chemoreceptors (nerves of the central nervous system), located in the medulla oblongata, monitor the pH levels of cerebrospinal fluid. When $CO_2$ from the plasma enters the cerebrospinal fluid, the pH of the fluid drop). In response to the decrease in pH, the central chemoreceptors stimulate the respiratory center to increase the inspiratory rate. Peripheral chemoreceptors (nerves of the peripheral nervous system), located in aortic bodies in the wall of the aortic arch and in carotid bodies in the walls of the carotid arteries, monitor the pH of the arterial blood. An increase in pH or $pCO_2$, causes these receptors to stimulate the respiratory center. Stretch receptors in the walls of bronchi and bronchioles are activated when the lungs expand to their physical limit. These receptors signal the respiratory center to discontinue stimulation of the inspiratory muscles, allowing expiration to begin. This response is called the

inflation (Hering-Breur) reflex. Autonomic breathing is not only controlled by metabolic demands but also constantly responds to changes in emotions,. Final respiratory output involves a complex interaction between the brainstem and higher centres, including the limbic system and cortical structures.

To be able to control and predict patient's breathing, it is important to view the time series signals from a new perspective by considering breathing as a dynamical system. Recently Tewatia (Tewatia *et al.*, 2011) published their findings based on analysis of randomly chosen breathing patterns of 16 patients. All 16 patients' breathing pattern were stationary and deterministic with presence of positive largest Lyapunov exponent (LLE) thus establishing that breathing pattern of lung cancer patients is not random or irregular rather deterministic in nature albeit chaotic. This helps in designing coaching and prediction methodologies based on their daily breathing pattern, potentially more accurate for longer latencies, which is explored in this thesis. In the second chapter we employed surrogate algorithms in order to establish the presence of chaotic determinism in a patient's breathing pattern. Once established, we have used several nonlinear state-space based methodologies for predicting breathing pattern of lung cancer patients which are presented in the third chapter. In the fourth chapter we took one step towards personalized medicine. In this part of the study we have used Recurrence Quantification Analysis (RQA) for analyzing individual breathing pattern. In this chapter we have shown how to assess the predictability and complexity of given breathing time series and choose different treatment methodologies based on quantification analysis. In the fifth chapter, we have worked on how chaos control algorithms based on nonlinear dynamical systems theory can be incorporated into this field to achieve control and have designed a methodology for coaching patients to be able to achieve favorable breathing pattern with more reproducibility for each treatment fraction. Each

of these sections are introduced below and explained in each chapter followed by the final chapter for conclusion and further studies. Most of the methods explained are implemented on time series obtained using RPM(Real-time Positioning Management, Varian Medical System, Palo Alto, CA) which tracks an infrared block placed on the chest. Mechanical coupling between the RPM surrogate and tumor motion cannot always be assumed and a correlation has to be developed and continuously monitored to be able to use the RPM surrogate directly for tumor tracking. However, the methods described below are applicable to any time-series data and can be directly translated to tumor co-ordinates once the technology is mature enough to provide real time tumor co-ordinates.

## 1.1 Surrogate testing of breathing patterns of lung cancer patients

Before using any tools from non-linear dynamics, it is important to establish presence of chaotic determinism in a patient's breathing pattern. State-of-the-art methods from the field of chaos theory, surrogate data testing methods, are employed to test the hypotheses if the origin of the waveform under consideration is a result of processes such as white noise, linear process passed through a nonlinear filter. Given a real random-like time series, the first question to answer is whether the data carry any information over time, i.e. whether the successive samples are correlated. Using standard statistical testing, the least interesting null hypothesis of white noise has to be rejected if the analysis of the time series should be of any use at all. Further, if nonlinear methods are to be used, the null hypothesis to be rejected is that the data involve only temporal linear correlations and are otherwise random. A statistically rigorous framework for such tests is provided by the method of surrogate data. The surrogate data, generated to represent the null hypothesis, are compared to the original data under a nonlinear discriminating statistic in order to reject or approve the null hypothesis. The surrogate data test for nonlinearity has become

popular in the last years, especially with regard to the null hypothesis that the examined time series is generated by a Gaussian (linear) process undergoing a possibly nonlinear static transform. This chapter describes the surrogate data test for the three hypotheses, i.e. linear filtered white noise, data passed through a nonlinear filter and pseudo periodic data. Some of the limitations and caveats of the test will be discussed and techniques to improve the robustness and reliability of the test will be reviewed.

## 1.2 Time series prediction of lung cancer patients' breathing pattern based on nonlinear dynamics and chaos theory

Prediction using regularized local linear methods has been employed and the prediction error using the state-space based methods have been compared to adaptive linear autoregressive prediction methods. This study focuses on predicting breathing pattern, which is crucial to deal with system latency in the treatments of moving lung tumors. Predicting respiratory motion in real-time is challenging, due to the inherent chaotic nature of breathing patterns, i.e. sensitive dependence on initial conditions. In this work, nonlinear prediction methods are used to predict the short-term evolution of the respiratory system for 62 patients, whose breathing time series was acquired using respiratory position management (RPM) system. Single step and N-point multi step prediction are performed for sampling rates of 5Hz and 10Hz. We compare the employed non-linear prediction methods with respect to prediction accuracy of Adaptive Linear Prediction (ALP) filters. A Local Average Method (LAM) and local linear methods (LLM) combined with a set of linear regularization techniques to solve ill-posed regression problems are implemented. For all sampling frequencies both single step and N-point multi step prediction results obtained using LAM and LLM with regularization methods are compared to ALP prediction filters for the selected patients.

## 1.3 Recurrence quantification analysis (RQA) of lung cancer patients' breathing pattern

Recurrence plots provide qualitative and quantitative information about breathing cycles even for short-time data series. In this section, Recurrence Quantification Analysis (RQA) is employed as a quantitative decision making tool to classify patients to be able to tailor personalized motion management treatment strategies. A fundamental property of deterministic dynamical systems and one typical for nonlinear dynamical systems is that states, i.e. trajectories, come arbitrarily close to one another after some time, which is also called recurrence of states. Eckmann et al. (Eckmann *et al.*, 1987) have introduced a tool, with which one can visualize the recurrence of states in state space. Recurrence plots represent such a sub-space and enable one to investigate an m-dimensional state space trajectory through a two-dimensional representation of its recurrences. In this chapter, we build and quantitatively analyze the breathing pattern acquired for seven healthy volunteers. We compute six Recurrence quantifiers for all volunteer data. We also establish relationship between the RQA parameters with the NRMSE prediction error computed using LAM model. We also introduce Time-Resolved RQAs for automatic detection of Unstable Periodic Orbit (UPO), which can be used to intelligently coach the patients to maintain a comfortable reproducible breathing pattern. We finally derive an invariant quantity (second-order Renyi entropy) which is an important parameter describing the rate of loss of information in the chaotic attractor. This invariant parameter can give a very strong insight into predictability of breathing patterns.

## 1.4 Novel methodology for chaos control in breathing patterns of lung cancer patients

Predicting respiratory motion in real-time is challenging, due to the inherent chaotic nature of breathing patterns, short-term prediction can however be achieved by non-linear state space based methodologies if an appropriate time delay and embedding is used. In addition, a much larger prediction horizon can be achieved is patients can be coached to closely follow a regular breathing pattern. Any chaotic system has in its invariant set embedded countless set of UPOs of arbitrarily high periods. In this section, we examine a well explored area of chaos control and design a methodology for coaching patients. We introduce an in-house built breathing acquisition module which is used for acquisition of breathing pattern and locating the Unstable Periodic Orbit using Recurrence plot strategies. We use this as a breathing guide and assess the impact of using this guide on a volunteer using RQA methodology. Use of return maps based on intercycle breathing period (IBP) to establish fixed point, stable and unstable manifolds is also explored on the volunteer training data. We then provide a strategy for realtime targeting algorithms which can be directly applied on breathing waveforms to achieve chaos control. We complete the section with future directions and conclusions.

## 1.5 References

Bortfeld T, Jokivarsi K, Goitein M, Kung J and Jiang S 2002 Effects of intra-fraction motion on IMRT dose delivery: statistical analysis and simulation *Phys. Med. Biol.* **47** 2203-20

Eckmann J P, Kamphorst S O and Ruelle D 1987 {Recurrence plots of dynamical systems} *EPL (Europhys. Lett.)* **4** 973-7

Ehler E and Tomé W 2008 Lung 4D-IMRT treatment planning: An evaluation of three methods applied to four-dimensional data sets *Radiotherapy and Oncology* **88** 319-25

Ehler E and Tomé W 2009 Temporal dose variation mitigation *Physics in Medicine and Biology* **54** 4311-24

Ehler E D, Nelms B E and Tome W A 2007 On the dose to a moving target while employing different IMRT delivery mechanisms *Radiother Oncol* **83** 49-56

Rybak I, Abdala A, Markin S, Paton J and Smith J 2007 Spatial organization and state-dependent mechanisms for respiratory rhythm and pattern generation. *Prog. Brain Res.* **165** 201-20

Tewatia D K, Tolakanahalli R P, Paliwal B R and Tome W A 2011 Time series analyses of breathing patterns of lung cancer patients using nonlinear dynamical system theory *Phys Med Biol* **56** 2161-81

van Herk M 2004 Errors and margins in radiotherapy *Seminars in Radiation Oncology* **14** 52-64

# Chapter 2.Surrogate testing of breathing patterns of Lung Cancer Patients

## 2.1   Introduction

Breathing is a neurophysiological process, controlled by the rhythmical centers which are not irregular or random (Rybak *et al.*, 2007). To be able to control and predict patient's breathing, it is important to understand these signals from a new perspective by considering breathing as a dynamical system. Establishing chaos in acquired time series signals is a problem that has been addressed in the physics literature at considerable depth over the last three decades. A direct approach is to test short time-series data sets for sensitive dependence on initial conditions, and existence of functions mapping precisely the past state of the system with the future. This was established in our background study with the presence of Largest Lyapunov Exponent (LLE) and determinism, respectively.

However, it has been shown that non-chaotic and some linear stochastic processes can generate time series data which mimic low dimensional chaos. Therefore, surrogate data testing has been advocated which provides a formal statistical test of a null-hypothesis, such that the data are generated from a linear stochastic process. The idea of surrogate data hypothesis testing is to generate a set of artificial surrogate time series that resemble the original data and still are consistent with the null hypothesis. A test statistic that is pivotal to deterministic chaos, like short-term nonlinear prediction or correlation dimension, is used to test both the surrogates and the original data. If the test statistic value for the data is different from the ensemble of values estimated for the surrogates, then one may reject the underlying null hypothesis as being the

likely origin of the data. If the test statistic value for the data is not distinct from that for the surrogates, then one may not reject the null hypothesis. Initially, surrogate methods were intended as a method to check the results of dimensional analysis against the possibility of misdiagnosing a purely random signal as deterministic chaos.

In this paper, we have implemented three popular methods of surrogate data for 16 patients and correlation dimension is used as the test statistic for hypothesis testing.

## 2.2   Materials and methods

Suppose $x$ are scalar samples acquired at times $t_i$ separated by a fixed time interval $t_s$, hence$t_i = t_0 + i.t_s$, yielding the scalar time series $S$

$$S = \{x_i\}_{i \varepsilon T}; T = \{1,2,...,N\} \qquad\qquad 2.1$$

Using the Takens' embedding theorem (Takens, 1981) a time delay embedding in a $m$-dimensional Euclidian space can be generated using the scalar time series $S$ that preserves the topological properties of the attractor. In particular, Takens' embedding theorem guarantees that if$m \geq 2d + 1$, the time delay reconstruction of the attractor formed by the $m$-dimensional state space vectors:

$$\boldsymbol{x}_i = \left(\boldsymbol{x}_{i-(m-1)\tau}, \boldsymbol{x}_{i-(m-2)\tau}, ..., \boldsymbol{x}_{i-\tau}, \boldsymbol{x}_i\right) \qquad\qquad 2.2$$

is topologically equivalent to the original attractor whose state space is $d$-dimensional. In equation 1, $x_i$ are the original scalar time series data points and "$\tau$" is the time delay. To estimate an optimal time delay, we have used the first local minimum of the mutual information function (Fraser and Swinney, 1986), since this yields an attractor reconstruction that is as open as possible.

We have used the method of false nearest neighbors (FNN) (Kennel *et al.*, 1992) that allows one to estimate the minimal number of dimensions necessary to "disentangle" the attractor. (Kennel *et al.*, 1992). The method is based on the assumption that an attractor of a deterministic dynamical system folds and unfolds smoothly with no sudden irregularities in its structure. A global false nearest neighbor analysis incrementally increases m until the number of false nearest neighbors approaches zero. False nearest neighbors are defined as sets of points that are very close to each other in dimension m = k but are not in dimension m = k +1. However, usually the time series data obtained using experimental techniques are contaminated by measurement noise and hence the dimension m + 1 may be regarded as optimum when the percentage of false neighbours for points in the m + 1 dimensional state space is less than a certain threshold which is set as an arbitrary number depending on the type of data one is dealing with.

The three popular algorithms proposed address the null hypotheses of: (1) independent and identically distributed (i.i.d) noise (Algorithm 0), (2) linearly filtered i.i.d. noise (Algorithm 1) and (3) a static monotonic nonlinear transformation of linearly filtered noise (Algorithm 2) (Theiler *et al.*, 1992; Schreiber, 1998; Schreiber and Schmitz, 2000). More recently, Small et al. (Small and Tse, 2002; Small *et al.*, 2001) outlined an improved algorithm known as pseudo-periodic surrogate (PPS) algorithm that preserves both stationarity and differentiability while testing a similar hypothesis.

1.  Algorithm 0 (Amplitude Randomized): These surrogates are generated by randomizing the order of the data in the original time series. The surrogates generated this way have the same rank distribution as the original data, but temporal correlation is lost and thus the surrogates provide a test of the hypothesis of independent and identically distributed (i.i.d.) noise.

2. Algorithm 1 (Phase Randomized): These surrogates generated by randomizing the order of the phases in the Fourier transform F(t) of the original time series data x(t). Randomizing the phases of F(t) destroys any non-linear structure of the original time series while preserving the linear correlations or power spectrum. The result is a realization of a stochastic process with the same mean, standard deviation, and autocorrelation as S(t).

3. Algorithm 2 (Amplitude Adjusted Fourier Transform): This method of surrogate data generation, also called Gaussian Scaled Randomization is the most popular method and surrogates generated using this mimic a linear stochastic process passed through a nonlinear filter. A set of random numbers with Gaussian distribution equal to the length of original time series x (t) is first generated. The random numbers are then rearranged into a series s (t) whose rank distribution is the same as the original time series. Similar to Algorithm 1, phase randomization of the Fourier transform of s(t) is performed to generate z(t). Finally, surrogate G(t) is obtained by reordering the original data x(t) to have the same rank distribution as z(t).

4. Pseudoperiodic surrogates (PPS): Stam et.al (Stam *et al.*, 1998) and others observed that Algorithm 2 (AAFT) does not perform well in presence of strong periodic components in the original time series data. This could be because of end-mismatch problem which has been addressed by several authors (Schreiber, 1998; Schreiber and Schmitz, 2000). Data exhibiting cyclic behavior are inconsistent with the hypothesis of "Static monotonic nonlinear transformation of linearly filtered noise". Small et.al. (Small *et al.*, 2001) have proposed a surrogate data generation method that preserves the periodic structure of the original data, but destroys the small scale structures of the time series, such as chaotic, linear and non-linear deterministic structure.  The algorithm for this method is as follows

a) Construct the vector delay embedding from the scalar time series x(t)

$$\tilde{x}_i = \left[ x_{i-(m-1)\tau}, x_{i-(m-2)\tau}, \ldots x_i \right]^T, i = 1 + (m-1)\tau, \ldots, N \ldots\ldots\ldots\ldots[2.3]$$

b) Using time series data from index 1 to $N$- $\tau_w$ where $\tau_w$ =m*($\tau$-1) is the window length.

c) Call this attractor A.

d) Choose an initial condition at random and call this $s_1$ . This is a vector with length $m$

$$s_1 \in \tilde{x}_i, i = 1 + (m-1)\tau, \ldots, N$$

e) Let i=1.Choose a neighbor$z_j \in A of s_i$, according to the probability distribution

$$Prob(z_j = z_t) \propto exp\left(\frac{-\|z_t - s_i\|}{\rho}\right) \qquad\qquad 2.4$$

f) Set $s_{i+1} = z_{j+1}$as a successor to $s_i$. Increment $i$.

g) Repeat step e and f till $i=N$.

The generated time series $(s_i)_1$is the surrogate time series. $(.)_1$ is the scalar first coordinate of the vector. The generated vector time series is a stochastic trajectory, or random walk on the original attractor A. Therefore, the surrogates generated using this algorithm follow the same vector field as the original data.  However, they are contaminated with dynamic noise which destroys the fine inter-scale dynamic behavior. The attractor A is reconstructed from the original time series using Taken's embedding theorem with an optimum value of $\tau$ and $m$ calculated using first minimum of the mutual information method and FNN method, respectively.   Selection of appropriate noise level, i.e. selection of $\rho$ is a key parameter in this method.   In this implementation, we choose a neighbor$z_j \in A$ of $s_i$ according to the probability distribution shown in Equation 2.4. If noise radius, $\rho$, is too small, then the surrogate thus generated will be identical to the original attractor A. If $\rho$ is too large, then the surrogate generated will be temporally uncorrelated and thus resemble i.i.d. noise.   We selected $\rho$ to be the value which maximized the number of short segments (length=2) that are

the same between the original time series and the surrogate. As shown by Small et.al (Small and Tse, 2002; Small *et al.*, 2001), the value of ρ thus selected provides the perfect balance between too much and too little noise.

**Test Statistic:** Several test statistics such as mutual information, LLE, higher order moments, non-linear prediction error and correlation dimension have been used to test a given hypothesis using surrogate data (Hegger *et al.*, 1999; Sugihara and May, 1998). We have used correlation dimension, shown to be a pivotal statistic (Theiler and Prichard, 1996), which is implemented using the correlation integral method introduced by Grassberger and Procaccia(Grassberger and Procaccia, 1983) as our test statistic of choice. The correlation dimension is an invariant measure of the attractor's fractal dimension i.e does not depend on how the attractor is reconstructed and it is the most popular among other similar fractal dimension measures, such as the information and box-counting dimension. We first start by calculating the correlation integral on the time series embedded in m-dimensional space.

$$C(r) = \frac{2}{N(N-1)} \sum_{i=1}^{N} \sum_{j=1}^{N} \Theta\big(\varepsilon - \|x_i - x_j\|\big) \qquad 2.5$$

Where $\Theta$ is the Heaviside step function $\Theta(x) = 0$ if $x \leq 0$ and $\Theta(x) = 1$ for $x > 0$. Correlation integral counts the number of pairs of points that are closer than the distance $\varepsilon$ to each other, and hence gives an estimate of the probability that the attractor trajectory visits a given region of state space. In fact the correlation dimension is a lower bound for the box counting dimension, which measures the number of "boxes" needed to cover a geometrical object. For small $\varepsilon$, $C(\varepsilon)$, scales as a power law and is proportional to $\varepsilon^D$. Correlation dimension is defined as

$$D = \lim_{\varepsilon \to 0} \lim_{N \to \infty} \frac{\partial \ln C(\varepsilon, N)}{\partial \ln \varepsilon} \qquad 2.6$$

The local slope of the graph of $\log(C(r))$ vs $\log(\varepsilon)$ is computed by the smooth derivative of $\log(C(\varepsilon))$ with respect to $\log(\varepsilon)$. Provided that the scaling $C(r) \sim \varepsilon^D$ exists at least for a

sufficiently large range of $\varepsilon$, a horizontal plateau of the local slope vs $\log(\varepsilon)$ should be formed for this range of $\varepsilon$. In real world applications, reliable estimation of D can be hard (meaning that the variance of the local slope is large) which indicates that there is no clear scaling. In this context, we would like to use this graph of local derivative of $C(\varepsilon)$ to differentiate the original data series from surrogate data series which is either linearly or non-linearly filtered noise or pseudo periodic data sets. For random data where the 'attractor' is in effect embedded within itself, the correlation dimension will obviously just reflect the embedding dimension used. Therefore, as we can never embed random data in a sufficiently high state space, the value of d(E) will rise to infinity with increasing E. For any other periodic or chaotic attractor, however, once the embedding dimension is substantially twice greater than the dimension of the attractor the value of d should remain constant, by the above arguments. 30 surrogate data sets were generated for the 16 patients under study using Algorithm 1, 2 and PPS

## 2.3    Results

Original time series and surrogate data generated using Algorithm 1 and Algorithm 2 and PPS is shown in Figure 2-1 (a) through (d).  Figures 2-2 (b ) through (c) shows a comparison of correlation dimension $d(\varepsilon_0)$ vs $\varepsilon_0$ for original and the surrogate data sets generated using Algorithm 1,2 and PPS algorithm. It can be seen that the correlation dimension for the surrogate data is clearly distinguishable from that of the original data.

Out of the 16 patient's studies, 2 patients with highly regular breathing cycles showed strong periodic orbits. The breathing signal of one of these patients is shown in Figure 2-3(a). The plot of the correlation dimension for original and surrogate data sets generated using Algorithm 1 and Algorithm 2 is shown in Figures 2-3(b) and 2-3(c) respectively, which clearly shows that we can reject the null hypothesis, meaning that the data is neither a linearly filtered i.i.d noise nor is it

generated from a linear noise process with a static non-linear filter. However, this does not test if the original data is periodic in nature. As shown in Figure 2-3 (d), the correlation dimension of original data cannot be distinguished from the pseudoperiodic surrogates, indicating that the original signal is mainly periodic in nature. Using the PPS method, one can clearly distinguish is the original signal is periodic or chaotic in nature.
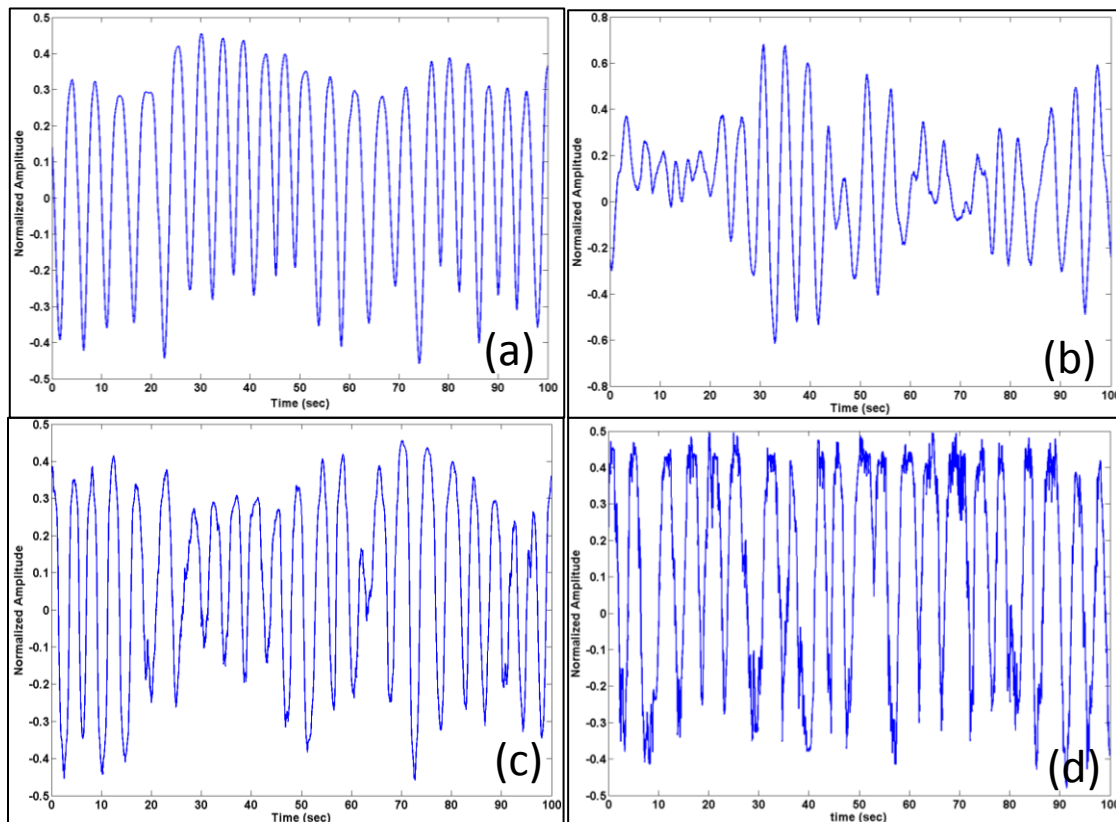


**Figure 2-1:** Original Time series and surrogate data generated using Algorithm 1 and Algorithm 2 and PPS is shown in figures (a) through (d) respectively.
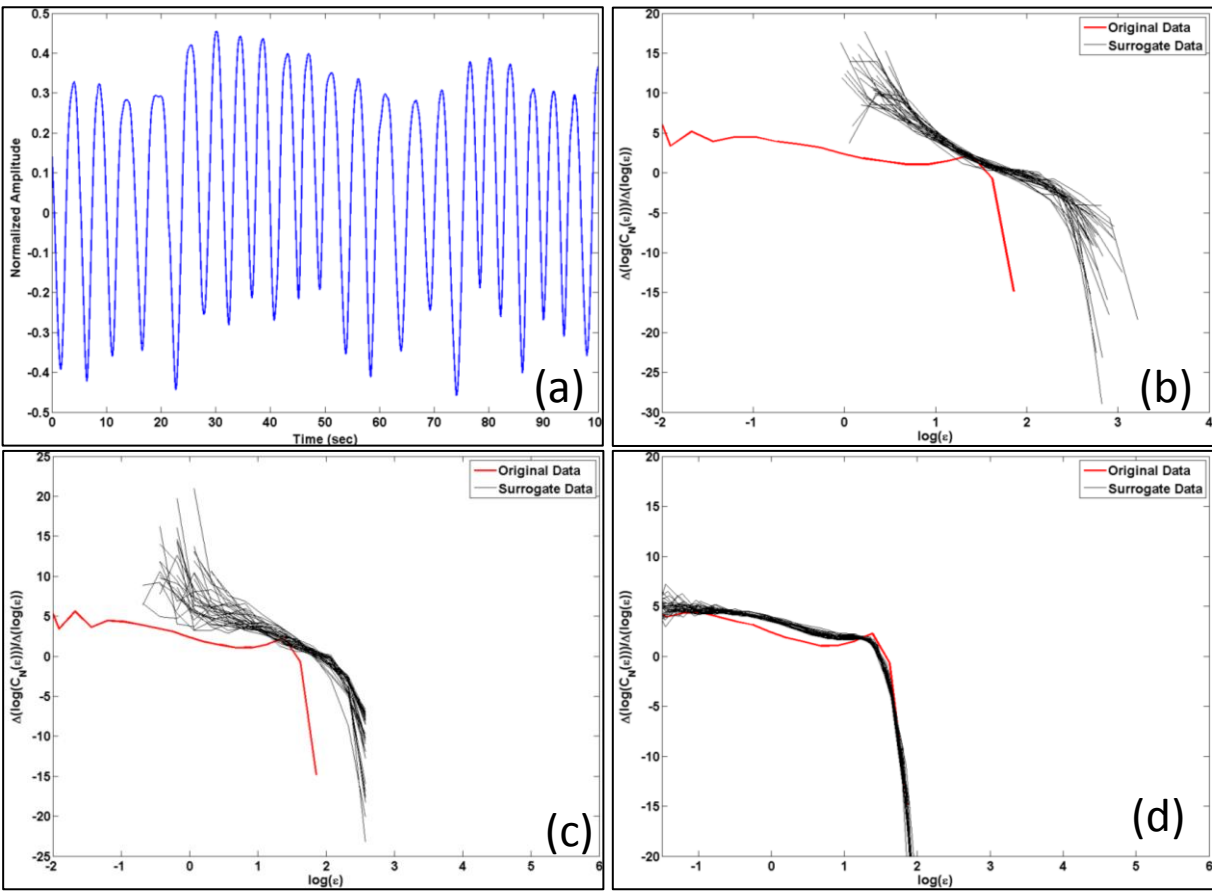
**Figure 2-2**: Original time series is displayed in figure (a) and comparison of correlation dimension generated using Algorithm 1 and Algorithm 2 and PPS is shown in figures (b) through (d) respectively.
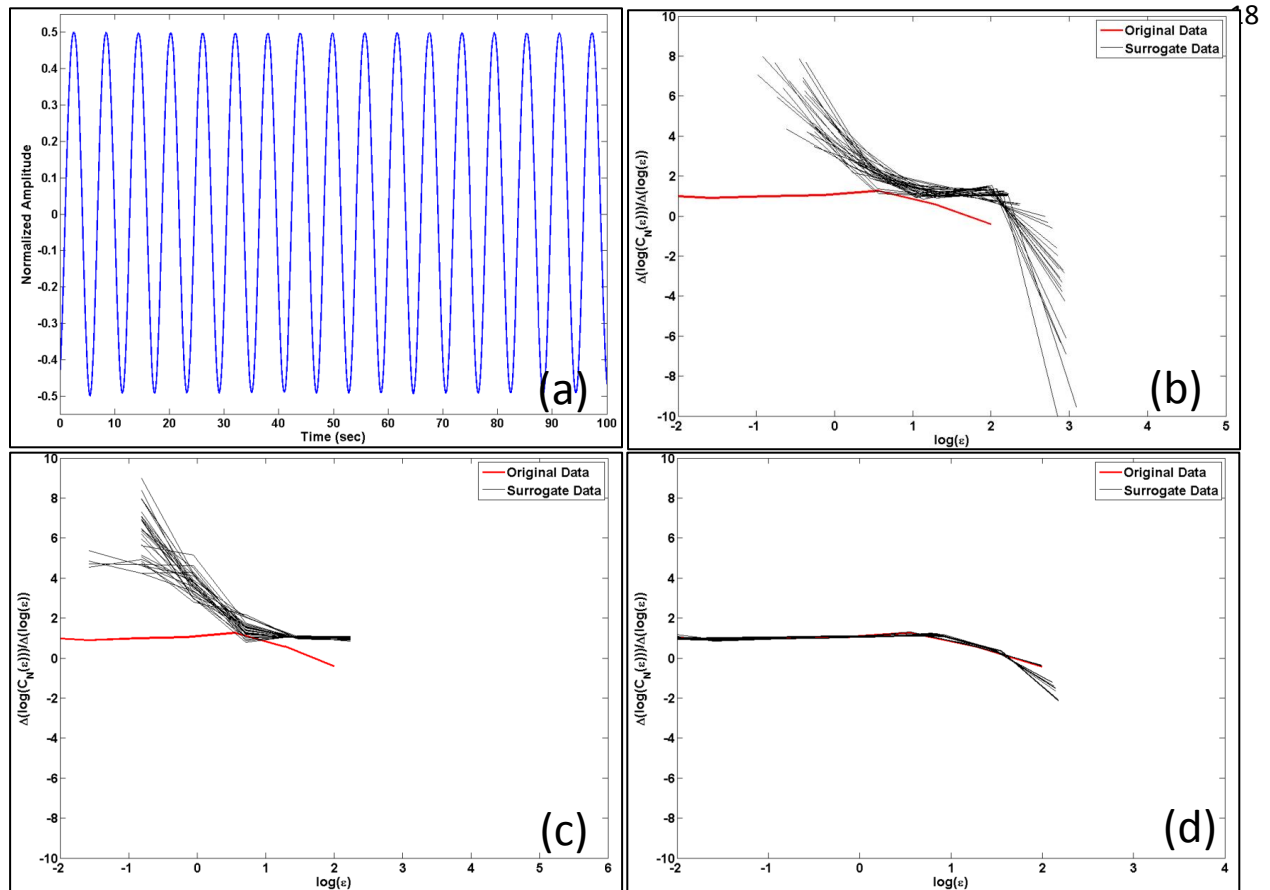
**Figure 2-3:** Original time series is displayed in figure (a) and comparison of correlation dimension generated using Algorithm 1 and Algorithm 2 and PPS is shown in figures (b) through (d) respectively. The PPS algorithm can identify periodic time series and hence the hypothesis that the time series has strong periodicity is not rejected.

## 2.4   Discussion

In order to avoid our data analysis to reflect our prejudice about the underlying system, we use surrogate data testing to find the least interesting explanation to represent a fair account of the structures that are present in the data that cannot be ruled out based on the data. It has been shown that non-chaotic and some linear stochastic processes can generate time series data which mimic low dimensional chaos. So, The idea of surrogate data hypothesis testing is to generate a set of artificial surrogate time series that resemble the original data and still are consistent with the null hypothesis .In this work, we, have implemented 3 different types of algorithms for

generation of surrogate data. We formulated 3 null hypotheses, to test if the data is generated from any of the following three processes namely: independent and identically distributed noise surrogate, Gaussians scaled linear noise passed through a nonlinear filter, and pseudoperiodic surrogate. We used correlation dimension, which is a invariant quantity as the test statistic to test the hypothesis. From the test cases, we found that time series of interest is clearly not generated from linear filtered i.i.d, linear noise passed through a nonlinear filter and is not a pseudoperiodic data set. The PPS algorithm is rather strong and was successful in identifying one patient with strong periodicity while the other two methods of surrogate data testing failed. Recognizing and establishing deterministic chaos in time series is an important step towards application of other nonlinear algorithms for prediction and control.

However, the computations for correlation dimension can be very intensive and takes an enormous amount of computation time and memory for calculation of $D_2$ for 30 surrogates. This analysis can be tested using the second order Renyi Entropy($K_2$), also an invariant quantity, introduced in Chapter 4 which can be calculated from Recurrence Plots and is comparatively less resource and time intensive than the box counting algorithm.

The work presented in this chapter reinforces the chaotic nature of breathing pattern and thus opens the way for nonlinear analysis and validates the use of promising techniques for prediction and control which are explored in the coming chapters.

## 2.5   References

Fraser A M and Swinney H L 1986 Independent coordinates for strange attractors from mutual information *Phys Rev A* **33** 1134-40

Grassberger P and Procaccia I 1983 Characterization of Strange Attractors *Physical Review Letters* **50** 346

Hegger R, Kantz H and Schreiber T 1999 Practical implementation of nonlinear time series methods: The [small-caps TISEAN] package *Chaos: An Interdisciplinary Journal of Nonlinear Science* **9** 413

Kennel M B, Brown R and Abarbanel H D I 1992 Determining embedding dimension for phase-space reconstruction using a geometrical construction *Physical Review A* **45** 3403

Rybak I, Abdala A, Markin S, Paton J and Smith J 2007 Spatial organization and state-dependent mechanisms for respiratory rhythm and pattern generation. *Prog Brain Res* **165** 201-20

Schreiber T 1998 Constrained randomization of time series data *Physical Review Letters* **80** 2105-8

Schreiber T and Schmitz A 2000 Surrogate time series *Physica D: Nonlinear Phenomena* **142** 346-82

Small M and Tse C 2002 Applying the method of surrogate data to cyclic time series *Physica D: Nonlinear Phenomena* **164** 187-201

Small M, Yu D and Harrison R 2001 Surrogate test for pseudoperiodic time series data *Physical Review Letters* **87** 188101

Stam C J, Pijn J P M and Pritchard W S 1998 Reliable detection of nonlinearity in experimental time series with strong periodic components *Physica D: Nonlinear Phenomena* **112** 361-80

Sugihara G and May R 1998 Nonlinear forecasting as a way of distinguishing chaos from measurement error in time series *Nonlinear physics for beginners: fractals, chaos, solitons, pattern formation, cellular automata, complex systems* 118

Takens F 1981 Detecting strange attractors in turbulence *Dynamical systems and turbulence* **898** 365-81

Theiler J, Eubank S, Longtin A, Galdrikian B and Doyne Farmer J 1992 Testing for nonlinearity in time series: the method of surrogate data *Physica D: Nonlinear Phenomena* **58** 77-94

Theiler J and Prichard D 1996 Constrained-realization Monte-Carlo method for hypothesis testing *Physica D: Nonlinear Phenomena* **94** 221-35

# Chapter 3.  Time series prediction of lung cancer patients' breathing pattern based on nonlinear dynamics

## 3.1  Introduction

Tumor motion caused by patient breathing creates challenges for accurate radiation dose delivery to a tumor while sparing healthy tissues. All respiratory-compensating methods developed or being investigated require predictive filters to compensate for system latencies. Combination of real-time imaging with a powerful prediction engine is a key to successful tumor motion management. The review article by Verma et.al presents mathematical models for all existing prediction algorithms that have been developed in the last decade. They summarize that all studies indicate that the predictions with long latency are error prone and aren't accurate enough to be implemented clinically (Verma *et al.*, 2011). With the advent of newer tumor tracking technologies such as the Calypso tracking system (Calypso, Seattle, Washington), RealEye<sup>TM</sup> Motion (Navotek Medical Ltd, Yokneam, Israel), or real time MR Radiotherapy systems like the one being developed by Viewray (Viewray Inc., Cleveland, OH) with which it will be possible to acquire real-time MR images at a frame rate of 4 images/sec the presented non-linear prediction methods can be directly implemented on the tumour motion coordinates. While linear predictive (LP) models, such as an infinite impulse response (IIR) prediction filters, have been employed with great success for short time horizon of the order of 50-200 ms for deterministic non-linear systems that exhibit sensitive dependence on initial conditions, their prediction however accurate, as shown in this work, deteriorates for N-point predictions for different sampling/imaging rates especially in the presence of measurement noise. We have already established that the breathing of lung cancer patients can be described as a 5 to 6

dimensional nonlinear, stationary and deterministic system that exhibits sensitive dependence on initial conditions, and hence any prediction models can only be used successfully for short time prediction horizon. The intended purpose of this chapter is to present different non-linear prediction algorithms by viewing the 1D time series as flow vectors generated from a multidimensional dynamical system. This is done by reconstructing the 1D time series in its true dimension by using time-delay embedding. We use nonlinear prediction methods to predict the time evolution of the breathing pattern for 62 lung cancer patients for a time ahead prediction horizon of 400 to 3000 ms. Both single step and N-point multi-step prediction are performed for sampling rates of 5 Hz and 10 Hz. We compare the employed non-linear prediction methods with respect to the prediction accuracy of an Adaptive LP (ALP) model employing an IIR prediction filter.

## 3.2 Materials and methods

### 3.2.1 State space representation

Scalar time series data of respiratory signals were obtained using the RPM system with a rate of 30 frames/sec. Suppose $x_i$ are scalar samples acquired at times $t_i$ separated by a fixed time interval $t_s$, yielding the scalar time series $S = \{x_i\}_{i \in T}; T = \{1,2,\ldots,N\}$. Using time delay embedding, the data can be represented in an m-dimensional state space as shown in equation (3.1), where $\tau$ is the embedding time delay and m is the embedding dimension.

$$\tilde{x}_i = \left( x_{i-(m-1)\tau}, x_{i-(m-2)\tau}, \ldots, x_{i-\tau}, x_i \right) \qquad 3.1$$

### 3.2.2 Adaptive Linear prediction model (ALP model)

A linear predictor is a system that predicts the future output signal as a linear function of a set of inputs (Sharp *et al.*, 2004; Vedam *et al.*, 2004). We consider linear predictors that are based on an AR (autoregressive) model, i.e that have the form

$$\hat{x}_{t+\Delta} = \sum_{j=1}^{SHL} a_j x_{t-(j).t_s}$$
$$\epsilon_{t+\Delta} = \hat{x}_{t+\Delta} - x_{t+\Delta}$$

3.2

Where $x_t$ is the amplitude of the scalar signal at time t, m is the order the AR model. The estimated signal at $\hat{x}_{t+\Delta}$ is therefore predicted as a linear combination of the known previous positions $x_t$ through $x_{t-j.ts}$. Note that the noise component has been suppressed, which for prediction purposes has to be averaged over leaving the AR part only. In case of adaptive linear AR prediction, the optimum set of coefficients $\{a_j\}_{j \in \{1..SHL\}}$ are continually found by minimizing the mean squared error ($\varepsilon_{t+\Delta}$) of predictions on a set of training samples based on the respiratory motion data collected 60 seconds prior, i.e. over a signal history length (SHL) of 60 seconds. Using the so determined optimum set of coefficients the breathing signal was predicted 400-3000 ms into the future.

### 3.2.3 Model free local prediction method in state space

The simplest form of local prediction is to consider the most similar segment of a given scalar time series in the past, or stated differently, one uses a nearest neighbor point, $\tilde{x}_{t_1}$ for some time index $t_1 < t-\tau$ in the past, to form $\tilde{x}_{t_{1+N}}$ in order to arrive at a prediction for the future time series point $N$-time steps ahead, $\tilde{x}_{t+N}$. The idea of analogies, i.e. finding similar segments of scalar time series data, is directly related to the property of recurrence of orbits of dynamical systems, which furnishes the theoretical underpinning for the use of local predictions (Kantz and Schreiber, 2004; Farmer and Sidorowich, 1987). Hence, the problem of predicting the future

value of $\tilde{x}_t$ $N$-time steps ahead is reduced to finding the nearest neighbor point to the point $\tilde{x}_t$ in the past and using it to estimate $\hat{x}_{t+N}$. Even if the original dynamics is chaotic, close orbits diverge only gradually and hence some degree of short-term prediction can be achieved using this method. However, if the reconstructed state space dimension is too low, then orbits starting from $x_t$ and its neighbors may not deviate as smoothly as the original orbits. Therefore, careful state space reconstruction is of immense importance for local prediction, and this does not simply rely on the selection of embedding dimension, m, but rather on the selection of embedding window length, $\tau_w$. The embedding window length $\tau_w = (m-1)\tau$ is the length of data segments on the trajectory of the underlying attractor. For a constant embedding window length $\tau_w$, state space reconstructions for varying m (adjusting $\tau$ accordingly, so that $\tau_w = (m-1)\tau$ is constant) are qualitatively the same (Kugiumtzis, 1996). The method described here can be further improved by taking the average of the mappings of the k nearest neighbors in the past, $\mathcal{N} = \{\tilde{x}_{t(1)}, \dots, \tilde{x}_{t(k)}\}$. This approach, also called the local average model (LAM) has limited prediction capability for sparse data, but for higher dimensional data it performs as well as other methods and sometimes better than the more advanced methods. For very noisy data, model free methods can work very well.

### 3.2.4  Functional approximation: Local Linear methods in state space

When building a local linear model one constructs an approximation of the tangent plane at a given target point $\tilde{x}_t$ as described in detail below. Local linear models (LLM) are linear autoregressive models that hold only for a region around the target point $\tilde{x}_t$ formed by the nearest neighbor points sometime in the past (Farmer and Sidorowich, 1987). The parameters are estimated by ordinary least squares (OLS) minimization and this usually requires that $k > m + 1$, where $k$ is the number of nearest neighbors used in the model and $m$ is the embedding dimension.

The prediction *N*-time steps ahead is then computed by evaluating the model equation for the target point, $\tilde{x}_t$. Note that the solution for the model parameters may be numerically unstable if k is close to m.

In local linear prediction with noisy data, the OLS solution can have large variance and regularization methods, designed to be more robust against noise, can provide better results. Regularization can be achieved by down weighting some or all of the singular directions by choosing filter factors less than 1 (cf. to equation 3.7). Two different types of regularization methods to the local linear models are implemented here and they are specified by the value of the so-called truncation parameter q. Assuming a current state $\tilde{x}_t$ , the task is to make N-time step ahead predictions.

1. The OLS solution for the parameters of the local linear model is regularized using principal component regression (PCR) (Kugiumtzis, 2002a; Kugiumtzis *et al.*, 1998) (Xie and Kalivas, 1997). PCR rotates the natural basis of local state space to match the basis formed by the principal components found using singular value decomposition (SVD) of the matrix formed by the nearest neighbor points. Then the space is projected onto the subspace formed by the first q principal axes, the solution for the parameters is then found in this subspace and it is transformed back to the original state space to yield the PCR regularized solution for the parameters. In this way, the estimated parameters have smaller variance (they are more stable) at the cost of introduced bias. Moreover, PCR may reduce the effect of noise. A necessary condition for the PCR solution is that *k* > *q* + *1*, so that stable solutions can be reached even when *m* > *k* provided that the truncation parameter is sufficiently small. The value of *q* is selected by minimizing the error between the predicted value and the actual value for the training data set.

2. Partial Least Squares (PLS): Strategies to select first few components using Principal Component Analysis (PCA) for the PCR technique use the input matrix only and do not take into account the output vector $y$. In contrast to PCR, PLS finds components of the input matrix that are also relevant to the output vector $y$. PLS regression uses a projection into the subspace spanned by the Krylov vectors, which are assumed to be linearly independent. Qualitatively, the PLS estimator shrinks the OLS estimate by taking into account not only the size of the singular values, but also the size of the Fourier coefficients. (O.C. Lingizerde and N. Christophersen, 1997).

We now embark on the detailed description of the methods described above and the algorithms associated with them. For data generated by a deterministic dynamical system, there exists a functional dependence of $x_{t+N}$ on $\tilde{x}_t$: $x_{t+N} = \mathcal{F}(\tilde{x}_t)$. The graph of the reconstructed dynamics for N-time steps ahead, $F^N$, is a smooth surface embedded in $\Re^{m+1}$. Around the local neighborhood of $\tilde{x}_t$, the surface may be locally approximated by the tangent plane, i.e. the linearization of $F^N$ at the center of mass of the neighbourhood around $\tilde{x}_t$,

$$
\begin{aligned}
y_t &= b^T x_t + \varepsilon_t^d \\
x_t = \tilde{x}_t - \bar{x}; \; y_t &= x_{t+N} - \bar{y}; \\
b^T &= \nabla F^N(\bar{x})
\end{aligned}
\qquad 3.3
$$

Where $x_t$ and $y_t$ are centered differences for $\tilde{x}_t$ and $x_{t+N}$ and $\nabla F^N(\bar{x})$ is the gradient of $F^N$ evaluated at $\bar{x}$.

## Algorithm:

**a)** Using the method of delays, the time series data is represented in a *m*-dimensional embedded space by delay vectors

$$
\tilde{x}_i = \left[x_{i-(m-1)\tau}, x_{i-(m-2)\tau}, \dots, x_i\right]^T, i = 1 + (m-1)\tau, \qquad 3.4
$$

**b)** Given a training subset $\mathcal{T}$ consisting of delay vectors, and a target point $\widetilde{\boldsymbol{x}}_t$ that is not included in $\mathcal{T}$, we are interested in the local linear prediction of $\widetilde{\boldsymbol{x}}_t$

**c)** Let $\widetilde{\boldsymbol{X}} = \left(\widetilde{\boldsymbol{x}}_{t(1)}, \widetilde{\boldsymbol{x}}_{t(2)}, \dots, \widetilde{\boldsymbol{x}}_{t(k)}\right)^T \in \mathfrak{R}^{k,m}$ be the k nearest neighbors of $\widetilde{\boldsymbol{x}}_t$ in $\mathcal{T}$, arranged in increasing order according to their distance from $\widetilde{\boldsymbol{x}}_t$. $\widetilde{\boldsymbol{X}}$ is a $k$ x $m$ matrix in which each row is given by a nearest neighbour point in the m-dimensional embedding space. Let $\widetilde{\boldsymbol{y}} = \left(x_{t(1)+N}, x_{t(2)+N}, \dots, x_{t(k)+N}\right)^T \in \mathfrak{R}^k$ be the response vector of length $k$ formed from the last components of the $k$ time advanced nearest neighbour vectors.

**d)** Let $\bar{\mathbf{x}}$ be the transpose of the row vector containing the averages of the $m$ columns of $\widetilde{\boldsymbol{X}}$ and $\bar{y}$ be average of the components of $\widetilde{\boldsymbol{y}}$

$$\bar{\mathbf{x}} = \begin{pmatrix} \frac{1}{k}\sum_{i=1}^{k} x_t^1(i) \\ \vdots \\ \frac{1}{k}\sum_{i=1}^{k} x_t^m(i) \end{pmatrix} \in \mathfrak{R}^m \qquad\qquad 3.5$$

$$\bar{y} = \frac{1}{k}\sum_{i=1}^{k} y(i) \in \mathfrak{R}$$

Then centered versions of the nearest neighbor matrix, $\widetilde{\boldsymbol{X}}$ and response vector $\widetilde{\boldsymbol{y}}$ of the matrix $\widetilde{\boldsymbol{X}}$ are obtained as follows: $\boldsymbol{X} = \widetilde{\boldsymbol{X}} - \mathbf{1}\bar{\mathbf{x}}^T$, and $\boldsymbol{y} = \widetilde{\boldsymbol{y}} - \bar{y}\mathbf{1}$, where $\mathbf{1}$ is a $k \times 1$ vector of ones. Furthermore, the centered versions of the target point and the response are given by: $\boldsymbol{x}_t = \widetilde{\boldsymbol{x}}_t - \bar{\mathbf{x}}$ and $y_t = x_{t+N} - \bar{y}$.

**e)** For prediction, the following model is then assumed for the centered versions of the response vector $\boldsymbol{y} = \boldsymbol{X}\boldsymbol{b} + \varepsilon$, where $\boldsymbol{b}$ is a vector of m unknowns and $\varepsilon$ is a random error with zero mean and covariance matrix $var(\varepsilon) = \sigma^2 \boldsymbol{I}$, where $\boldsymbol{I}$ is a $k$ x $k$ identity matrix. It

has been shown that $b$ only weakly depends on noise and hence the noise component can be safely ignored in the following steps. (Kugiumtzis *et al.*, 1998)

**f)** For the prediction estimation of $X$, the following Singular Value Decomposition (SVD) of $X$ is assumed.

$$X = U\Sigma V^T, UU^T = I, V^T V = I$$
$$\Sigma = diag(\sigma_1, \sigma_2, \dots \sigma_r) \tag{3.6}$$

Where $r \leq min(k, m)$ is the rank of $\mathbf{X}$ *and* $\sigma_1 > \sigma_2 > \cdots > \sigma_r$ are the ordered non-zero singular values of $X$. The columns of $U$ *and* $V$ span the r-dimensional range spaces $R(X) \subset \Re^k$ and $R(X^T) \subset \Re^m$, respectively. *R(X)* is commonly referred to as the signal space.

**Prediction estimators:**

**g)** Once $X \in \Re^m, y \in \Re^k$ are computed, for a given centered target point $x_t \in \Re^m$, the prediction estimator for the centered response $y_t$ is defined by $\hat{y}_t \equiv \hat{\mathbf{b}}^T x_t$, where $\hat{\mathbf{b}}$ is an estimate for **b**. Here, we consider estimators for **b** that have the following form

$$\hat{\mathbf{b}} = V\Sigma^{-1}\Lambda U^T y = \sum_{i=1}^r \frac{\lambda_i}{\sigma_i}(u_i^T y)v_i, where \; \Lambda = diag(\lambda_1, \dots, \lambda_r) \tag{3.7}$$

In fact equation (3.7) encompasses most of the well-known regularization estimators, differing only their choice of the filter factor matrix $\Lambda$. (Kugiumtzis, 2002b; Kugiumtzis *et al.*, 1998)

Ordinary Least squares regression (OLS): The OLS regression estimate, $\hat{\mathbf{b}}_{OLS}$, is found by minimizing the $l_2$-norm of the quadratic equation, $\min_{\mathbf{b}} \|y - X\mathbf{b}\|_2^2$ and $\hat{\mathbf{b}}_{OLS}$, can be estimated as follows:

$$\hat{\mathbf{b}}_{OLS} = X^{\dagger}y = V\Sigma^{-1}U^{T}y = \sum_{i=1}^{r} \frac{1}{\sigma_i}(u_i^{T}y)v_i \qquad\qquad 3.8$$

where $X^{\dagger} \equiv V\Sigma^{-1}U^{T}$ denotes the generalized Moore-Penrose pseudo-inverse of $X$. This estimator is obtained from equation 3.7 by setting the filter factors $\lambda_i = 1 \ for \ i = 1, 2, \ldots, r$. This amounts to allowing all directions of $R(X)$ spanned by the columns of $U$ to contribute to the OLS regression estimate.

*Principal Components regression (PCR):* On the other hand, the PCR regression estimate uses a subspace of R(X) spanned by the first few columns (q<r) of U and the filter factors are chosen such that $\lambda_i = 1 \ for \ i = 1,2,\ldots, q$ and $\lambda_i = 0 \ for \ i = q + 1, \ldots, r$. The rationale for this approach is that the last r-q columns of U are assumed to be on the order of the noise level, and hence do not provide any additional information about the true $y$ and $\mathbf{b}$. In this study, we have used *q=r-2* for all the breathing patterns considered.

*Partial Least Squares regression (PLS):* PLS regression uses a projection into the subspace spanned by the Krylov vectors to estimate $\hat{\mathbf{b}}_{PLS}$. The Krylov vectors are assumed to be linearly independent and are given by equation (3.9)

$$XX^{T}y, (XX^{T})^{2}y, \ldots, (XX^{T})^{q} \qquad\qquad 3.9$$

Let us denote by $K$ the $k$ x $q$ matrix formed using the $q$ Krylov vectors as columns. The matrix K is then used to define the following operator:

$$P = K(K^{T}K)^{-1}K^{T}$$

One can easily verify that $P^2 = P$, and hence $P$ defines a projection operator into the subspace spanned by these q linearly independent Krylov vectors. Using this projection operator the partial least square estimator for $\mathbf{b}$ can be written as follows:

$$\hat{\mathbf{b}}_{PLS} = X^{\dagger}Py \qquad\qquad 3.10$$

Qualitatively, the estimator shrinks the OLS estimate by taking into account the size of singular values as well as the size of Fourier coefficients.

## 3.2.5 Prediction Error Estimator

To validate the predictive power of a model, the available data set is split into two parts, one for fitting and one for testing. Cross-validation procedures could be used here as well. The normalized root mean squared error (NRMSE), computed on all points in the test set, can be used to measure the quality of prediction. A value of close to 1 for the NRMSE means that the prediction is as good as the mean value prediction whereas a value of 0 is indicative of a perfect prediction. The *N*-step time prediction error can be measured using NRMSE as follows:

$$NRMSE = \sqrt{\frac{(1/(M-N-n))\sum_{t=n+1}^{M-N}(x_{t+N}-\hat{x}_{t+N})^2}{(1/M)\sum_{i=1}^{M}(x_i-\bar{x})^2}} \qquad\qquad 3.11$$

Where $\bar{x}$ is the sample mean of the data, $x_{t+N}$ for *t= n+1, ... ,M-N*, are the response values of the test set, and *n* denotes the number of time series points in the training set.

For both the model free and local linear prediction method, the number of nearest neighbors (*k*) and the radius of neighborhood around the target point are two of the main parameters. In the current work the number of neighbors has been fixed to 5 for all patient breathing pattern considered and the radius of neighborhood was varied from 0.02 to 0.2 units to achieve this. The success of the prediction with PCR and PLS relies heavily on the proper selection of the regularization parameter, q. For PLS and PCR, cross-validation (CV) techniques are commonly used, in which the effect of the shrinkage parameter q on a measure such as Root Mean Square Error (RMSE) is evaluated (Lukas, 1998). Other methods for estimation of q, include finding a threshold value that represents the noise variance of the time series signal or by placing a

condition that singular values account for at least some proportion of the total data variation in X. In this study, the value of q was chosen as r-2 for both PCR and PLS techniques by qualitative analysis of the predicted signals.

## 3.3   Results

The methods described above have been applied to the breathing patterns of 62 patients. The data set for each patient was divided into a training set and a testing set consisting. The length of the training set was varied from 10 to 200 sec, depending on the total length of breathing cycle collected for a particular patient, yielding for a sampling rate of 5 Hz, 10, Hz, and 30 Hz values of n varying between 50, 100, 300 to 1000, 2000, 6000  respectively. Prediction for all breathing patterns was done using the ALP method and the space methods discussed above, i.e. the LAM, LLP: OLS, PLS and PCR algorithms. The length of prediction for N-step prediction was varied from 400 ms to 3000 ms for 5 Hz and 10 Hz sampling rates. Among the 62 patients selected randomly, we found 9 patients where the NRMSE of the nonlinear methods were not significantly better than ALP. Retrospectively, we present the data for 62 patients binned into separate groups, hereafter referred to as Bin1 and Bin2. Bin 1 consists of 50 prediction cases where the state-space methods are significantly better than ALP, especially for longer prediction times whereas Bin 2 consists of 12 patients, further divided into Bin 2a and Bin2b. Bin 2a consists of 9 patients where prediction by either method does not yield an adequate prediction of the breathing pattern since all prediction models depend mainly on the history of the signal, i.e. prediction of a breathing pattern that does not repeat itself to some extend in the observation window cannot be successfully or accurately predicted. However, if the breathing pattern were to be observed for a very long time, accurate predictions can be made, however, this can be impractical for radiation therapy applications. Bin 2b consists of 3 patients for which both non-

linear prediction and the adaptive linear prediction methods performed equally well, since their breathing was highly regular.

Figure 3-1 shows the predicted signal for one of the patients in the Bin1 (Patient 1) using LAM, OLS, PLS, PCR prediction methods that are contrasted to the ALP prediction for 1000 ms ahead. It can be seen that all state-space based regularized prediction methods perform better than the ALP model. Furthermore, Figure 3-1 shows that the LAM performs as well as other model based regularized prediction methods. It can be clearly seen from Figure 3-1 that the ALP-model fails for multi time step prediction of $N$-time steps ($N > 1$). It is important to note that most studies in the literature involve only single time-step prediction for different imaging rates/sampling rates (5-30 Hz). We find that the state-space based methods for multi time-step prediction for the two imaging rates (10 Hz and 5 Hz) yield a better predication than the ALP model. Figure 3-2 shows the full signal and predicted signal for one of the patients in Bin1 (Patient 2) using only 18 seconds of breathing for training of both nonlinear and linear prediction methodologies. It can be seen that nonlinear methods perform well in spite of the short training period. The NRMSE for the above two patients for all methods for 1000ms prediction at both 10 Hz and 5 Hz sampling rate is tabulated in Table 3-1. Histogram plot for all patients in Bin1 for 2 sec prediction time at 5Hz and 10 Hz is shown in Figure 3-3(a) and Figure 3-3(b) respectively. The mean NRMSE as a function of prediction time for all the 50 patient signals in Bin1 is shown in Figure 3-3 (c) for both 10 Hz and 5 Hz sampling rates.
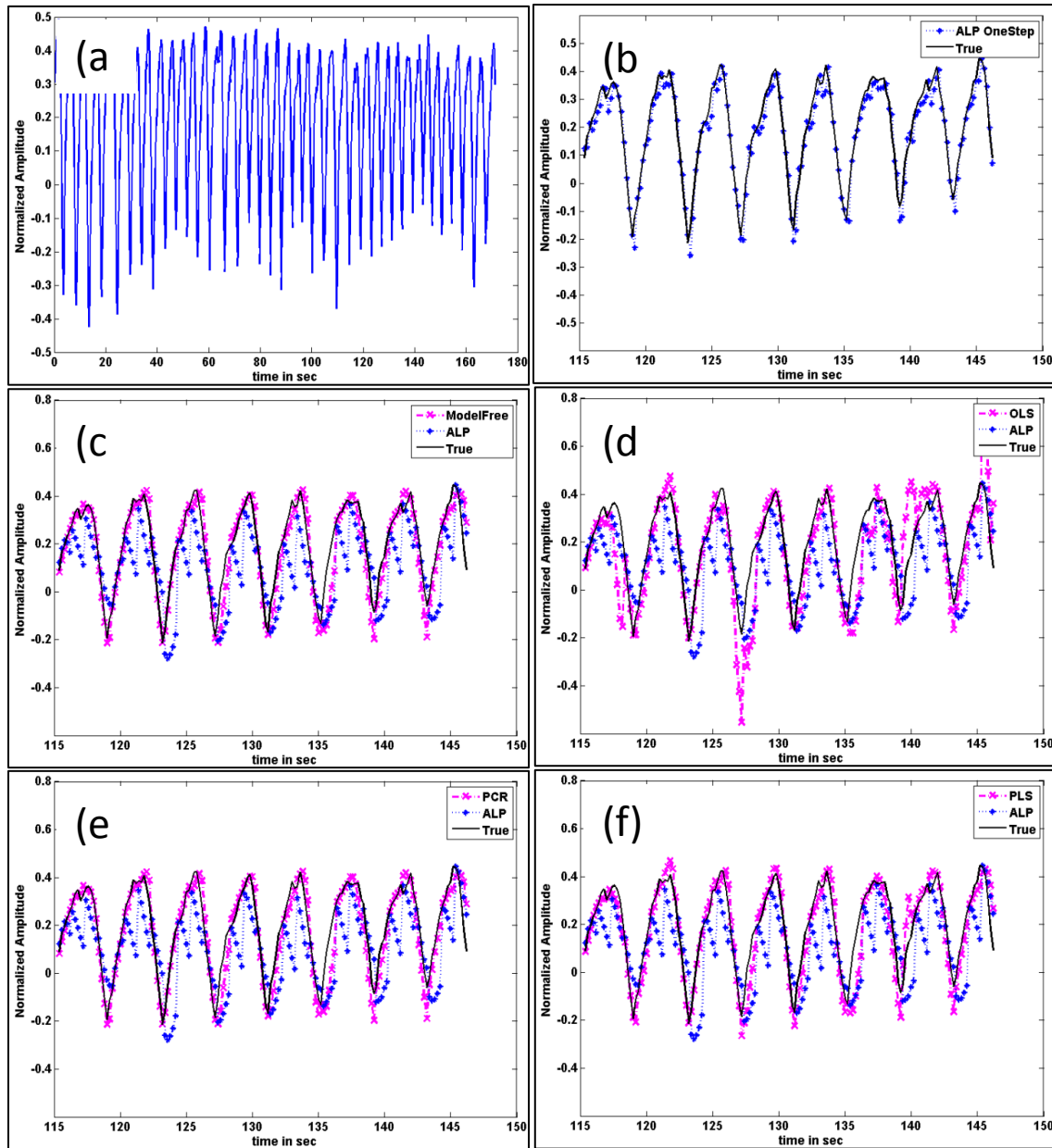
**Figure 3-1:** 5 time steps ahead prediction for the Patient 1 with Respiratory Cycle shown in (a) predicted with (b) ALP-OneStep (0.32) (c) LAM (0.37) (d) OLS (5.66), (e) PCR (0.37), and (f) PLS (0.39) are compared with the ALP model (0.63). The numbers in parenthesis are the respective NRMSEs. Signals were predicted 1000 ms ahead employing a sampling frequency of 5Hz
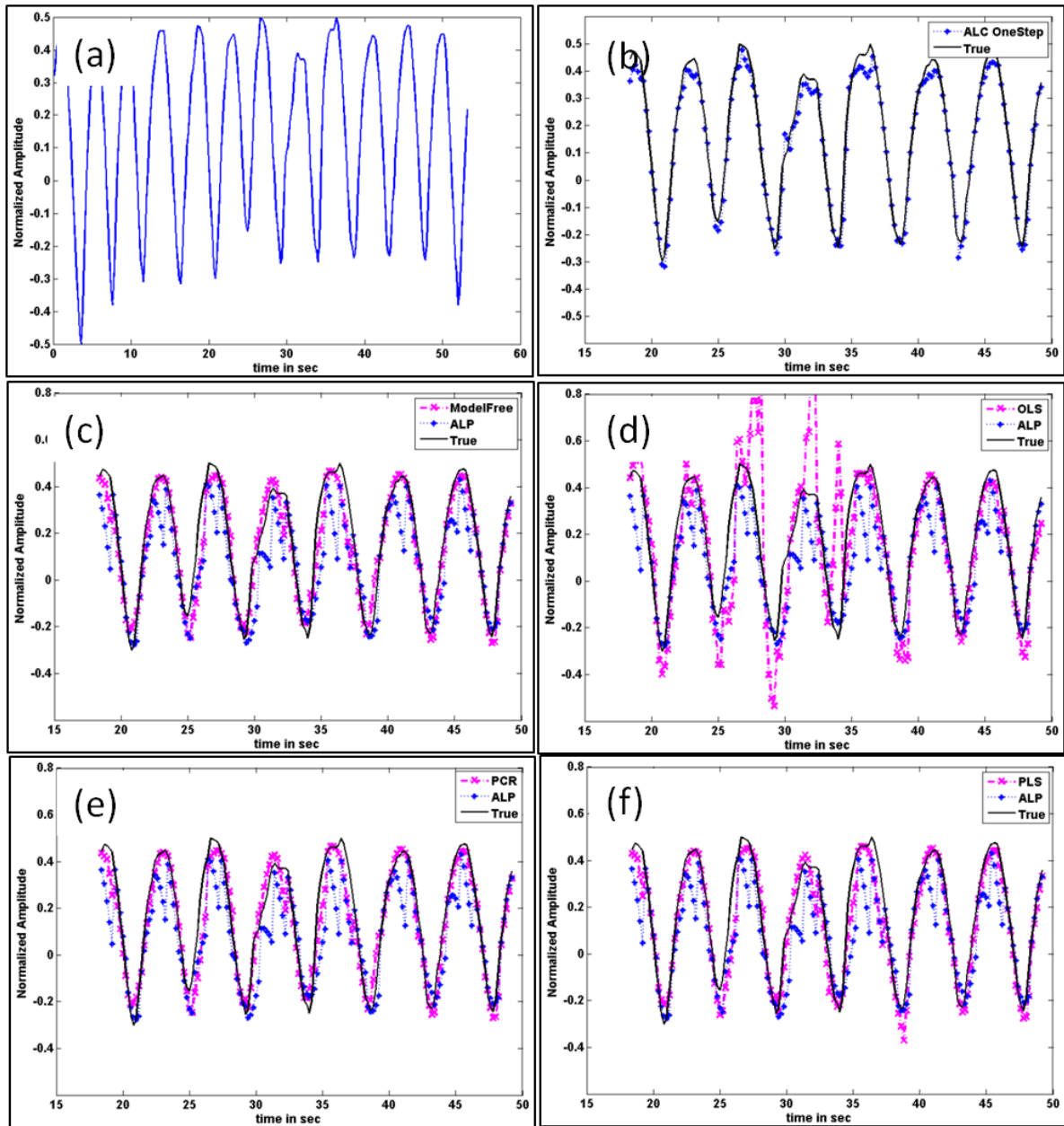
**Figure 3-2:** 5 time steps ahead prediction for the Patient 2 with Respiratory Cycle shown in (a) predicted with (b) ALP-OneStep(0.17) (c) LAM (0.34) (d) OLS(43.96), (e) PCR(0.32), and (f) PLS(0.34) are compared with the ALP model(0.56). The numbers in parenthesis are the respective NRMSEs. Signals were predicted 1000 ms ahead employing a sampling frequency of 5Hz.
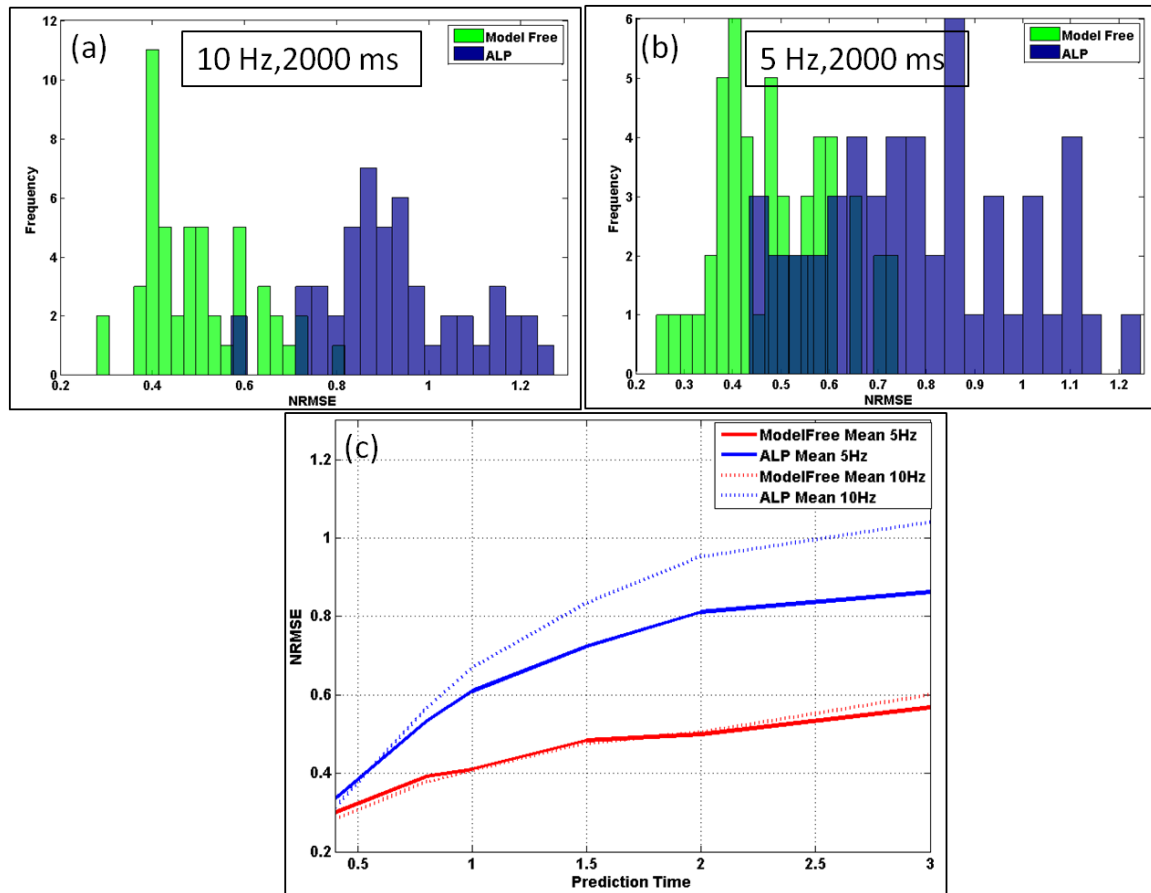
**Figure 3-3:** Histogram distribution for all patients in Bin 1 predicted with LAM (Green) and ALP prediction(Blue) for 2000 ms prediction at (a) 10 Hz (b) 5 Hz  is shown. 3-.3 (c) shows NRMSE as a function of Prediction Time for LAM (Red) and ALP (Blue) at 10 Hz(dotted) and 5 Hz (solid) sampling rates.

Figure 3-4(a) and 3-4(b) shows the complete cycle and predicted signal for one of the patients in Bin2a (Patient 3) for LAM and ALP methods for 1000ms ahead prediction.  It can be seen that both methods are unable to yield an adequate prediction of the breathing pattern for the patient shown in Figure 3-4(a).   Histogram plot for 9 patients in Bin2a for 2000ms prediction time at 5Hz and 10 Hz is shown in Figure 3-5(a) and Figure 3-5(b) respectively. The mean NRMSE as a function of prediction time for all the 9 patient signals in Bin2a is shown in Figure 3-5 (c) for 10

Hz and 5 Hz sampling rates. Figure 3-6(a) and 3-6(b) shows the complete cycle and predicted signal for one of the patients in Bin2b for LAM and ALP methods for 1000ms ahead. It can be seen that both methods perform equally well for the patient 4 shown in Figure 3-6(a).
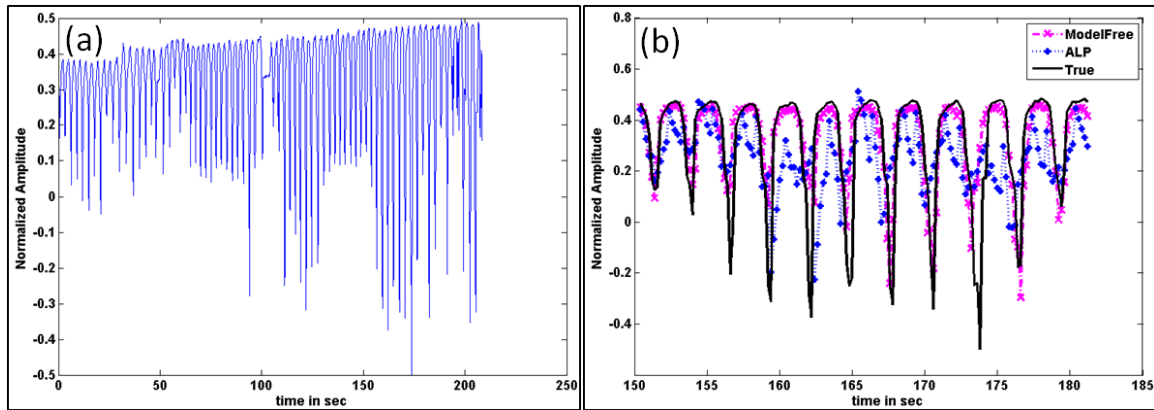


**Figure 3-4:** 5 time steps ahead prediction for the Patient 3 with Respiratory Cycle shown in (a) predicted with (b) LAM (0.93) is compared with the ALP model (1.58). The numbers in parenthesis are the respective NRMSEs. Signals were predicted 1000ms ahead employing a sampling frequency of 5Hz.
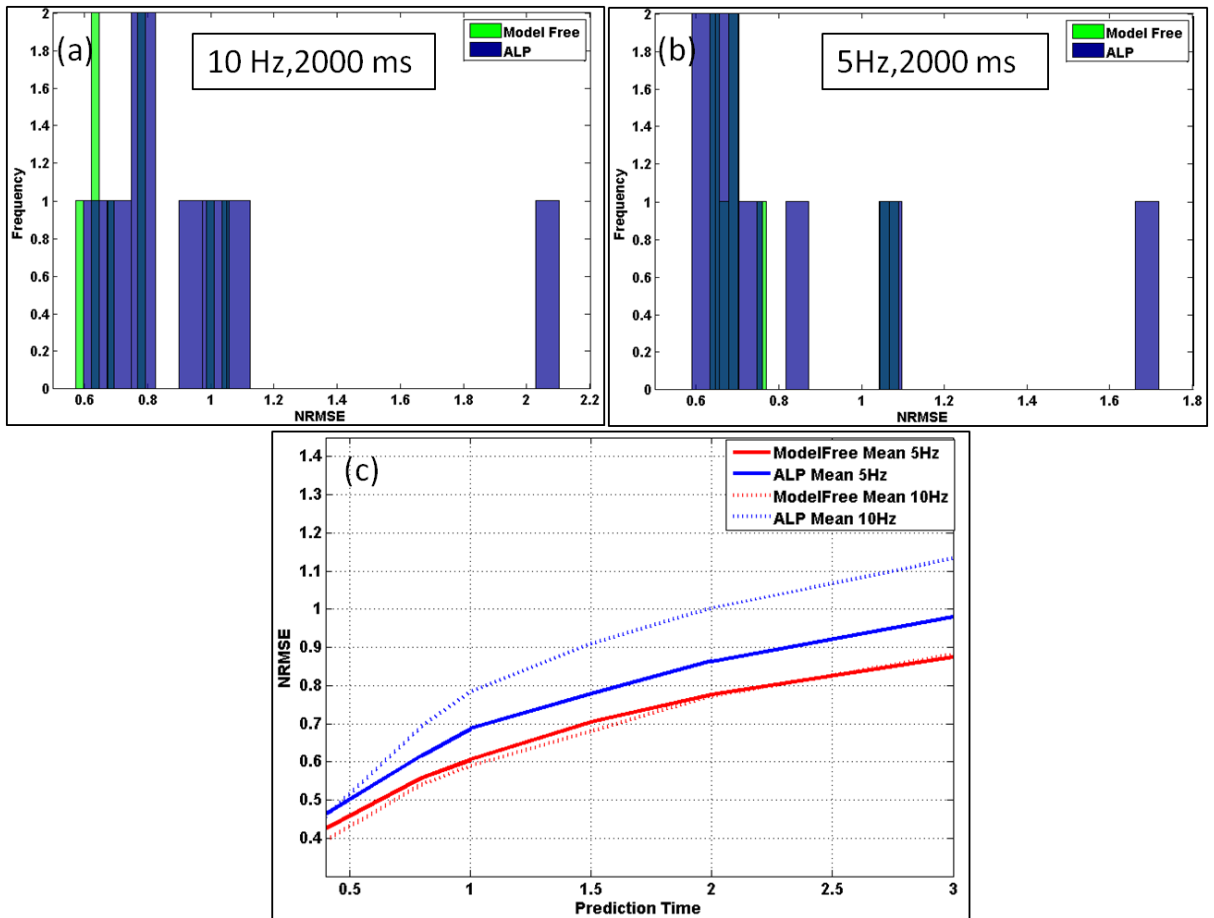
**Figure 3-5:** Histogram distribution for all patients in Bin 2a predicted with LAM (Green) and ALP prediction(Blue) for 2000 ms prediction at (a) 10 Hz (b) 5Hz  is shown. 3.5(c) shows NRMSE as a function of Prediction Time for LAM (Red) and ALP (Blue) at 10 Hz(dotted) and 5 Hz (solid) sampling rates.
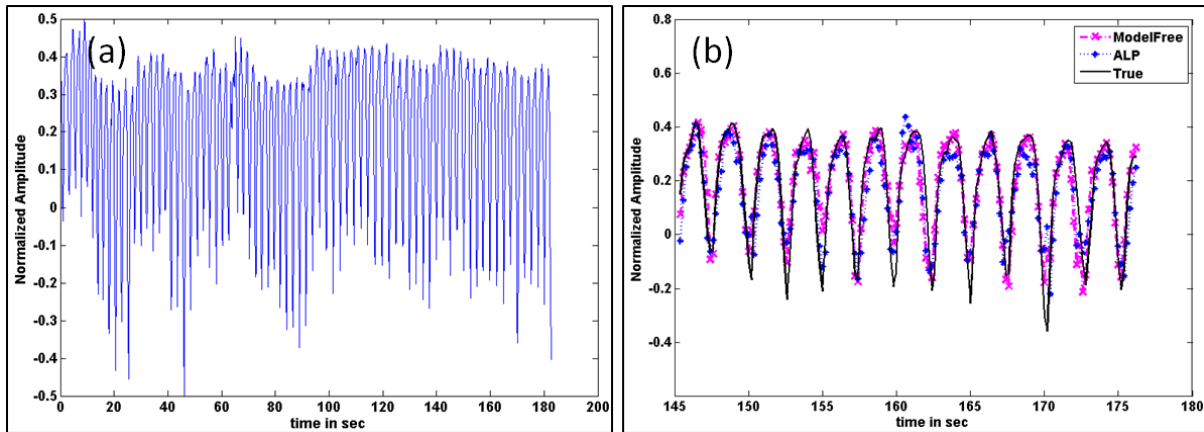
**Figure 3-6:** 5 time steps ahead prediction for the Patient 4 with Respiratory Cycle shown in (a) predicted with (b) LAM (0.43) is compared with the ALP model (0.49). The numbers in parenthesis are the respective NRMSEs. Signals were predicted 1000 ms ahead employing a sampling frequency of 5Hz.

| Prediction Time(sec) | 0.4 | 0.8 | 1 | 1.5 | 2 | 3 |
|---|---|---|---|---|---|---|
| **Adaptive Linear Prediction (ALP): 5Hz (10Hz)** | | | | | | |
| **Patient 1** | 0.33(0.29) | 0.56(0.52) | 0.63(0.56) | 0.85(0.75) | 0.97(0.93) | 1.1(1.07) |
| **Patient 2** | 0.26(0.25) | 0.49(0.49) | 0.56(0.59) | 0.81(0.73) | 0.94(1.03) | 1(1.05) |
| **Patient 3** | 1.56(1.56) | 1.70(1.87) | 1.56(1.83) | 1.78(2.17) | 1.72(2.10) | 1.81(2.26) |
| **Patient 4** | 0.40(0.51) | 0.47(0.94) | 0.49(1.05) | 0.50(1.19) | 0.50(1.26) | 0.57(1.32) |
| **LAM Prediction: 5Hz (10Hz)** | | | | | | |
| **Patient 1** | 0.31(0.27) | 0.36(0.34) | 0.37(0.37) | 0.44(0.43) | 0.47(0.53) | 0.52(0.57) |

| Patient 2 | 0.22(0.22) | 0.26(0.26) | 0.31(0.34) | 0.34(0.36) | 0.40(0.42) | 0.50(0.52) |
|-----------|------------|------------|------------|------------|------------|------------|
| Patient 3 | 0.84(0.80) | 0.97(0.88) | 0.93(0.91) | 1.05(0.99) | 1.05(1.00) | 1.3(1.22) |
| Patient 4 | 0.27(0.30) | 0.38(0.39) | 0.43(0.35) | 0.4(0.40) | 0.5(0.46) | 0.54(0.58) |

**Table 3-1**: NRMSE for different prediction times is listed for the sample patients 1-4.

## 3.4   Discussion

Robust implementation of any lung tumor motion management technique solely depends on goodness of breathing pattern prediction because of system latency issues. Exactness of results obtained based on linear or nonlinear prediction methodologies are based how closely our used methodology is able untangle the actual dynamics of the given system. From the cohort of patients studied, our results indicate that $N$-step ahead non-linear prediction methods yield better prediction results than an $N$-step ahead adaptive linear autoregressive prediction model (cf. Figures 3-3 and 3-5). Hence, we may consider that the use of non-linear prediction methods for prediction the breathing pattern of lung cancer patients may lead to improved, robust and accurate long-term prediction that can be used to account for system latencies. It is well known that variations in breathing pattern, during the course of treatment, are a major cause for the changing intrafraction tumor motion trajectory.  Thus, currently, many research groups are developing or have developed prediction engines in order to maneuver the moving tumor during radiation therapy. The error in prediction due to the sensitive dependence on initial conditions for all the algorithms can be estimated. This error estimation is more closely related to  prediction horizon in the field of nonlinear chaotic dynamics and is nothing but an estimate of how far into the future one can predict a signal for a given error threshold. It has been shown that a prediction

engine based on nonlinear dynamics has a larger prediction horizon than other methods if an appropriate time delay and embedding dimension are chosen, which can be seen by the results presented for patients in Bin1. Proper time delay and embedding dimension allows one to reconstruct an attractor in which the presence of false nearest neighbors that can lead to incorrect prediction is minimized (Arslan Basharat, 2009; Kantz and Schreiber, 2004).

In our multi time-step prediction using local state space methods, the NRMSE is comparable to or better than well-established single time-step prediction using the ALP-model. Among, the local space methods, it can be seen that LAM performs as well as the LLMs. It has been shown that Local linear models with OLS work well with noise free or low noisy data (Kugiumtzis *et al.*, 1998). When  measurement noise is present, $X$ tends to be better conditioned. However, the prediction capability of OLS deteriorates because the part of the OLS solution that relates the directions masked with noise does not contain any useful information that can be used to predict the future signal.  It can be seen from the results in this study that OLS does not perform as good as regularized prediction methodologies PCR and PLS, which have performed equivalently on our measured data.

With the advent of newer tumour tracking technologies such as the Calypso tracking system (Calypso, Seattle, Washington), RealEye[TM] Motion (Navotek Medical Ltd, Yokneam, Israel), or real time MR Radiotherapy systems like the one being developed by Viewray (Viewray Inc., Cleveland, OH) with which it will be possible to acquire real-time MR images at a frame rate of 4 images/sec the presented nonlinear prediction methods can be directly implemented on the tumour motion coordinates. It can be seen that performance of an ALP model is frequency dependent and deteriorates at 10 Hz, and this is mainly due to the presence of noise which contributes to the determination of model parameters.  However, performance of the LAM and

LLP models are not frequency dependent since they do not significantly worsen for either sampling rate (see Figures 3-3 and 3-5). Thus, based on the cohort of patient breathing patterns analyzed for this study, the local state-space prediction models will be more desirable for prediction of real-time tumor coordinates; specifically LAM models, since they are computationally inexpensive and thus are more desirable.

The work presented in this paper can be extended in several ways for tracking tumor motion in real time. One can, for example, model breathing pattern based on neurophysiologic mechanisms. Another possibility is to use chaotic dynamics to control and guide patients breathing for regularity and reproducibility.

## 3.5   References

Arslan Basharat a M S 2009 Time Series Prediction by Chaotic Modeling of Nonlinear Dynamical Systems. In: *International Conference on Computer Vision*

Farmer J D and Sidorowich J J 1987 Predicting chaotic time series *Physical Review Letters* 59 845

Kantz H and Schreiber T 2004 *Nonlinear time series analysis*: Cambridge Univ Pr)

Kugiumtzis D 1996 State space reconstruction parameters in the analysis of chaotic time series-- the role of the time window length *Physica D: Nonlinear Phenomena* 95 13-28

Kugiumtzis D 2002a State space local linear prediction *Modelling and Forecasting Financial Data, Techniques of Nonlinear Dynamics*  95–113

Kugiumtzis D ed 2002b *State space local linear prediction*

Kugiumtzis D, Lingjaerde O and Christophersen N 1998 Regularized local linear prediction of chaotic time series *Physica D: Nonlinear Phenomena* 112 344-60

O.C. Lingizerde and N. Christophersen 1997 Shrinkage Properties of Partial Least Squares,.

Sharp G C, Jiang S B, Shimizu S and Shirato H 2004 Prediction of respiratory tumour motion for real-time image-guided radiotherapy *Phys Med Biol* 49 425-40

Vedam S S, Keall P J, Docef A, Todor D A, Kini V R and Mohan R 2004 Predicting respiratory motion for four-dimensional radiotherapy *Medical Physics* 31 2274-83

Verma P S, Wu H, Langer M P, Das I J and Sandison G 2011 Survey: Real-Time Tumor Motion Prediction for Image-Guided Radiation Treatment *Computing in Science & Engineering* 13 24-35

Xie Y-L and Kalivas J H 1997 Local prediction models by principal component regression *Analytica Chimica Acta* 348 29-38

# Chapter 4.  Recurrence Quantification Analysis of lung cancer patients' breathing pattern

## 4.1   Introduction

Clinically "real-time" tracking of tumor motion where the treatment can be actively and variably adapted in concordance with intrafractional changes is made available in the Cyberknife (Accuray, Sunnyvale, CA) (Shirato *et al.*, 2000; Seppenwoolde *et al.*, 2007; Nuyttens *et al.*, 2006).   Another commercially available system is the three- or four-dimensional Calypso electromagnetic tracking system (Varian Medical Systems, Palo Alto, CA) (Sawant *et al.*, 2009). Many authors have recognized the importance of identifying patients suitable for advanced 4D treatment methodologies. Mechalakos et al. examined treatment plans for 12 patients receiving radiation therapy for NSCLC. They found that the dose to 95 %( D95) of the gross tumor volume (GTV), changed on an average by only 1.4% when normal breathing effects were incorporated. However, with "heavy breathers," the D95 changed by almost 10%. Therefore, they conclude that patients with a large respiratory motion could have significant effects, and thus these patients should be identified (Mechalakos *et al.*, 2004).   The simplest measure would be to distinguish patients based on the extent of tumor motion. Gomez et al. (Gomez and Chang, 2011) in their review paper state that at their institution, in patients whose tumor motion is less than 1 cm, a "free-breathing" technique is typically used, with the creation of an ITV or iGTV and radiation treatment delivery in all phases of the breathing cycle. If the target volume moves more than 1 cm and the patient can breathe reproducibly, then radiation is either timed with certain phases of the breathing cycle while the patient breathes freely, or the patient is instructed to hold

their breath while radiation is delivered at deep inspiration (DISB). They also utilize visual and/or audio feedback guidance for patients who can comply with these devices.

The phrases that call for our attention are "regularity or reproducibility of breathing" and "compliance of patients for coaching". Based on these key parameters, one could use patient specific approaches to design 4D treatments. A basic flowchart elucidating this concept is shown in figure 1. Measures to quantify the regularity and reproducibility of breathing should be investigated and we will attempt to do so using recurrence plot methodologies based on nonlinear dynamics. We have investigated the usefulness of Recurrence Plots (RP) in previous work (Tewatia *et al.*, 2011). RPs are a 2D projection of a higher dimensional state space that represents how close states are to one another in a m-dimensional state space. Here we will extend our previous work using Recurrence Quantification Analysis (RQA), which uses quantifiers to measure predictability and complexity of breathing patterns. In the current work, we use the RPM system as a surrogate motion indicator although the results and methods developed here are also applicable to other technologies such as the Calypso electromagnetic tracking system (Varian Medical Systems, Palo Alto, CA) , the RealEyeTM Motion tracking system (Navotek Medical Ltd, Yokneam, Israel), or real time MR Radiotherapy systems like the one being developed by Viewray (Viewray Inc., Cleveland, OH) and Philips (Philips, Eindhoven, Netherlands). We discuss the methods employed in some detail in section 4.2. In section 4.3 we report on the results we have obtained using volunteer RPM data. In section 4.4 we discuss the implications of our findings and point to possible future directions this work could engender.
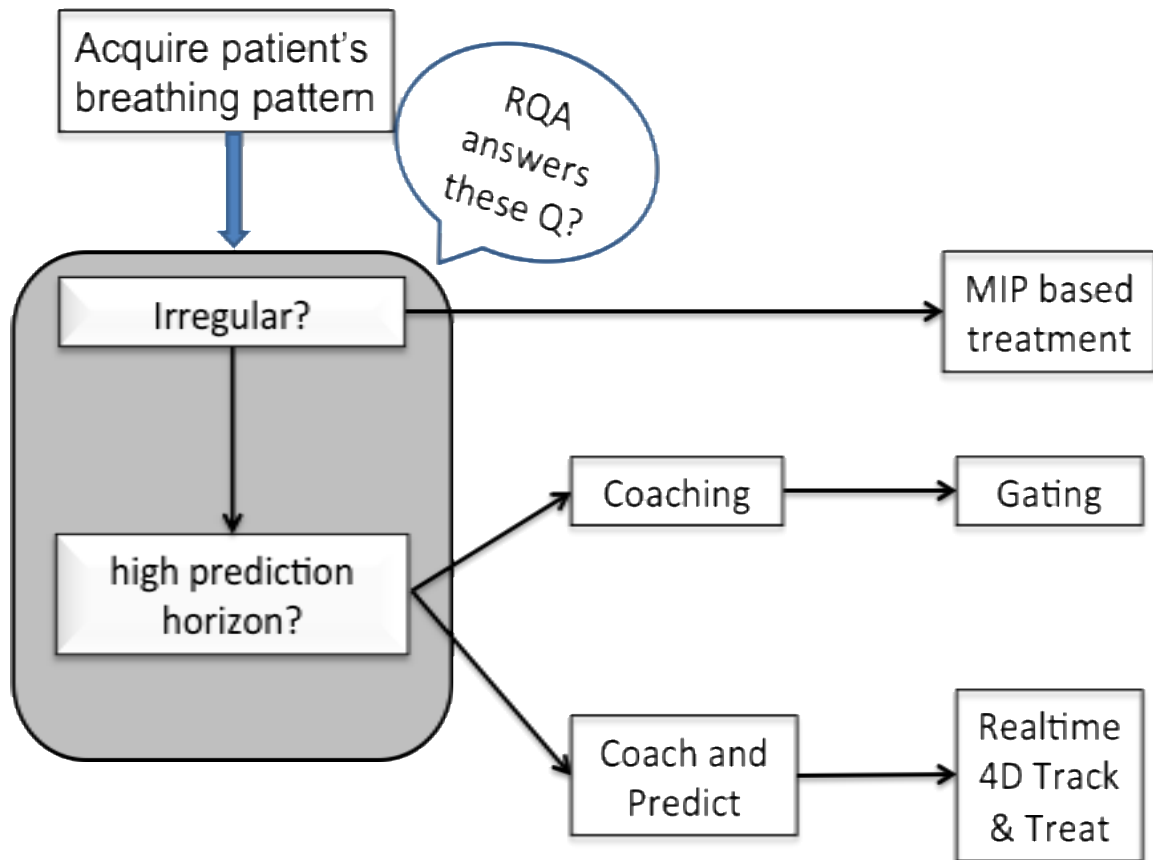
**Figure 4-1:** Flowchart showing a decision tree for 4D treatment strategy using Recurrence plot based on nonlinear dynamics.

## 4.2   Methods and Material

### 4.2.1  State space representation

A fundamental property of deterministic dynamical systems and one typical for nonlinear dynamical systems is that states, i.e. trajectories, come arbitrarily close to one another after some time, which is called recurrence of states. Eckmann et al. (Eckmann *et al.*, 1987) have introduced a tool, with which one can visualize the recurrence of states $x_i$ in state space. A reconstructed state space does not always have a dimension that is low enough so that a graphical representation of the attractor trajectory is possible. To visualize higher dimensional state spaces

(*m* > 3) one can project them into special two or three-dimensional subspaces. Recurrence plots represent such a subspace and enable one to investigate an m-dimensional state space trajectory through a two-dimensional representation of its recurrences.

Recurrence of a state at time *i* at a different time *j* is marked within a two-dimensional square matrix in which both rows and columns represent time. The pixel (*i, j*) represents the Euclidean distance between the two corresponding trajectory points. This representation is called a recurrence plot (RP). In an unthresholded RP (UTRP), the pixel having coordinates (*i, j*) is grey-shaded according to the numerical value of the Euclidean distance between the points  and  in a thresholded RP (TRP), the pixel having coordinates (*i, j*) is black if the distance falls within a specified threshold corridor and white otherwise.

The thresholded RP can be mathematically expressed as follows

$$R_{i,j} = \theta\big(\varepsilon - \|x_i - x_j\|\big), x_i \in \Re^m, i, j = 1, \dots N \qquad\qquad 4.2$$

Where N is the number of points considered, $\varepsilon$ is the threshold distance, $\|\bullet\|$ denotes the Euclidean norm and $\Theta$ is the Heaviside function. The purpose of RPs is the visual inspection of higher dimensional state space trajectories. Recurrence Plots exhibit characteristic large scale and small-scale patterns, the former were denoted by Eckmann et al. (Eckmann *et al.*, 1987) as typology and the latter as texture. Recurrence plots exhibit characteristic large-scale and small-scale patterns that are caused by the dynamical behavior of the non-linear system being studied e.g., diagonals (similar local evolution of different parts of the trajectory) or horizontal and vertical black lines (state does not change for some time).

The localization and quantification of Unstable Periodic Orbits (UPOs) for chaotic attractors is very important, since the attractor a chaotic non-linear system is the closure of all its UPOs. A trajectory of a non-linear dynamical system can be regarded as jumping from one UPO to the

next. RPs can be used to localize UPOs in a chaotic time series (Bradley and Mantilla, 2002). When the trajectory of the system comes close to an UPO, it stays in its vicinity for a certain time interval, whose length depends on how unstable the UPO is. This is reflected in the RP, as the pattern corresponding to periodic movement and consists of uninterrupted equally spaced diagonal lines.

Zbilut and Webber (Zbilut *et al.*, 1998) have developed recurrence quantification analysis (RQA) to quantify an RP. They have defined measures using the recurrence point density and the diagonal structures in the recurrence plot, the recurrence rate, determinism, the average and maximal length of diagonal structures, and entropy. A computation of these measures in small windows moving along the main diagonal of the RP yields the time dependent behavior of these variables and, thus, makes the identification of transitions in the time series possible. The RQA measures are based for the most part on the distribution of the length of the diagonal structures in the RP. In this work respiratory time series signals were obtained from seven volunteers for a length of 15 minutes using the RPM system, and were analyzed quantitatively using RQA.

### 4.2.2 Measure of complexity

The simplest measure, called the Recurrence Rate (RR) is a measure of the density of recurrence points, i.e. is the ratio of the number of recurrent states measured with respect to all possible states.

$$RR(\varepsilon) = \frac{1}{N^2} \sum_{i,j=1}^{N} R_{i,j}(\varepsilon) \qquad\qquad 4.3$$

The threshold $\varepsilon$ was chosen for all breathing patterns such that the RR was equal to 1%.

In this work, we consider the measures based on diagonals lines only, although the vertical line distribution has been extensively used in certain applications (Marwan *et al.*, 2007). Since $\varepsilon$ is finite, more line diagonals can occur directly below and above the Line of Identity (LOI) for

high resolution data. Therefore, diagonal lines in a small corridor around the LOI correspond to the tangential motion of the state space trajectory, but not to different orbits. Hence, this corridor is excluded for the estimation of all measures. In this study, we chose to exclude the corridor of a width to the Theiler window constraints, w= (m-1) τ.

***Determinism:*** Stochastic processes have very few short diagonals while deterministic processes have many long diagonals. Thus the percentage of recurrent points forming line segments parallel to the main diagonal is an indirect measure of determinism or predictability of the system. The threshold $l_{min}$ was set to 4.

$$DET = \frac{\sum_{l=l_{min}}^{N} lP^{\varepsilon}(l)}{\sum_{l=1}^{N} lP^{\varepsilon}(l)} \qquad\qquad 4.4$$

Where $P^{\varepsilon}(l)$ is the probability to find a diagonal line of at least length $l$.

***Average Diagonal Length:*** Diagonal lines in the RP represent co-moving segments of different parts of the trajectory. The longer the trajectories move within a $\varepsilon$-tube, the longer the diagonal lines in the RP will be. Thus, the length of these lines is an indirect measure of the divergence of the segments. The average diagonal line length is the average time that two segments of the trajectories that are close to each other and can be interpreted as the mean prediction time. The average diagonal length is given by

$$L_{avg} = \frac{\sum_{l=l_{min}}^{N} lP^{\varepsilon}(l)}{\sum_{l=l_{min}}^{N} P^{\varepsilon}(l)} \qquad\qquad 4.5$$

***Divergence (DIV):*** $L_{max}$ , the length of the longest diagonal or its inverse , the divergence (DIV) is related to the largest positive Lyapunov exponent.

$$L_{max} = max\{l_i; i = 1..N\}; DIV = \frac{1}{L_{max}} \qquad\qquad 4.6$$

Higher the divergence, more chaotic the orbit. For predicting the state of a given set of points, one could use points in the ε neighbourhood that are temporally in the past. In the presence of more than one point in the neighbourhood, their average is used for prediction. From the recurrence plots, one can see that a large nonlinear prediction error is introduced for states at the end of a diagonal line. Hence, long diagonal lines lead to better forecasting with average lengths of line denoting the prediction horizon.

***Entropy***: The measure entropy refers to the Shannon entropy of the frequency distribution of the diagonal lengths. It reflects the complexity of the deterministic structure in the system.

$$ENTR = -\sum_{l=l_{min}}^{N} p(l) \ln p(l) \; with \; p(l) = \frac{P^\varepsilon(l)}{\sum_{l=l_{min}}^{N} P^\varepsilon(l)} \qquad\qquad 4.7$$

## 4.2.3  Time Resolved RQA

It would certainly be feasible to perform recurrence quantifications within the entire window ($W_{large}$ = 20,000 represented by the single, large, outer Recurrence Matrix (RM) square. On the other hand the data can be windowed into forty smaller and overlapping RM squares ($W_{small}$ = 2000 points). In the latter case the window offset of 500 points means the sliding window jogs over 500 points between windows. Two effects are at play here. First, larger windows focus on global dynamics (longer time frame) whereas smaller windows focus on local dynamics (shorter time frame). Second, larger window offsets yield lower time resolution RQA variables, whereas smaller window offsets yield higher time-resolution variables. The above mentioned RQA variables are computed (extracted) from each RM (or RP). By implementing a sliding window design, each of those variables is computed multiple times, creating six  new derived dynamical systems expressed in terms of *%RR, %DET, $L_{Avg}$, $L_{Max}$, DIV* and *ENTR*. Alignment of those variables (outputs) with the original time series (input) (adjusting for the embedding dimension, *M)* might reveal details not obvious in the 1-dimensional input data.

### 4.2.4  Nonlinear prediction and relation to RQA parameters

Nonlinear prediction based on the model free state-space prediction method was implemented on the collected volunteer breathing data. The model free state-space prediction method is the simplest form of local prediction and amounts to finding similar segments of scalar time series data (Kantz and Schreiber, 2004; Kugiumtzis, 2002). Hence, we predict the future value of $\tilde{x}_t$ N-time steps ahead by finding and taking the average of the forward propagation of k nearest neighbors of $\tilde{x}_t$ in the past to estimate $\tilde{x}_{t+N}$. If the reconstructed state space dimension is too low, then orbits starting from $x_t$ and its neighbors may not deviate as smoothly as the original orbits. Hence, the state space was reconstructed very carefully. This methodology known as local average model (LAM) has been implemented for the volunteer data. Initially, 300 seconds of data was used for non-linear prediction of the subsequent 300 seconds and the size of the input data set was increased moving forward in time. To validate the predictive power of a model, the available data set is split into two parts, one for fitting and one for testing. The normalized root mean squared error (NRMSE), computed on all points in the test set, can be used to measure the quality of prediction. A value of close to 1 for the NRMSE means that the prediction is as good as the mean value prediction whereas a value of 0 is indicative of a perfect prediction. The N-step time prediction error was computed using NRMSE as shown in equation 4.8:

$$NRMSE = \sqrt{\frac{(1/(M-N-n))\sum_{t=n+1}^{M-N}(x_{t+N}-\hat{x}_{t+N})^2}{(1/M)\sum_{i=1}^{M}(x_i-\bar{x})^2}} \qquad 4.8$$

Where $\bar{x}$ is the sample mean of the data, $x_{t+N}$ for t= n+1, ... ,M-N, are the response values of the test set, and *n* denotes the number of time series points in the training set. The NRMSE for all volunteers was plotted against the calculated RQA parameters.

## 4.2.5 Invariant Measures

As described, the above mentioned RQA parameters vary with time. However, it is important to calculate invariant measures that are typical to the dynamical system under consideration. In this section, we first define the generalized Rényi entropy (Thiel *et al.*, 2004) .Consider an attractor *A* in a bounded *d*-dimensional space and suppose that the system is measured at time interval $\tau$. An attractor *A* provides a global picture of the long-term behaviour of a dynamical system but a more refined representation is given by the probability measure on *A*, which describes how frequently a given trajectory falls within some particular region of the phase space. Specifically, a state space can be divided into a set of N ($\varepsilon$) disjoint boxes $\Phi_i$ in order to determine with which frequency a trajectory visits these boxes. Each trajectory visits a sequence ($\phi_{il}, \phi_{i2} \ldots \ldots \phi_{im}$) of boxes where $i_j$ is a number in [$1 \ldots \ldots N (\varepsilon)$].We denote by p($i_l, i_2 \ldots \ldots i_m$) the joint probability of finding this trajectory at time $\tau$ in box $\phi_{i_1}$, at time $2\tau$ in box $\phi_{i_2}$., and so on. Using this joint probability distribution the "q-entropy" can be defined as follows:

$$K_q = -\lim_{\tau \to 0} \lim_{d \to \infty} \frac{1}{\tau d} \frac{1}{q-1} \ln \sum_{i_1..i_d} p^q (i_1 \ldots, i_d) \qquad 4.9$$

Second-order Renyi entropy (correlation entropy) is then defined as

$$K_2 = -\lim_{\tau \to 0} \lim_{d \to \infty} \frac{1}{\tau d} \ln \sum_{i_1..i_d} p^2 (i_1 \ldots, i_d) \qquad 4.10$$

This measure quantifies how fast the number of possible future evolutions increases with time. If the system is perfectly deterministic, there is only one possible trajectory it evolves in. Hence, there exists only one series of future steps with probability 1 and therefore, $K_2$=0. In contrast, one can easily show that for purely stochastic systems, the number of possible future trajectories increases to infinity so fast, that $K_2 \to \infty$ (Thiel *et al.*, 2004). Chaotic systems are characterized by a finite value of $K_2$, as they belong to an intermediate category. They are less predictable than purely periodic systems, but more predictable than purely stochastic systems. Also in the chaotic

case the number of possible trajectories diverges but not as fast as in the stochastic case. The inverse of $K_2$ has units of time and can be interpreted as the mean prediction horizon/time of the system.

$K_2$ is a lower bound of the Kolmogorov-Sinai (KS) entropy and is often used as its estimate, since it can be extracted from experimental time series data using the Grassberger and Proccacia (GP) algorithm (Grassberger and Procaccia, 1983a) for calculating the correlation integral $C_d(\varepsilon)$. $K_2$ is related to the correlation integral as follows.

$$C_m(\varepsilon) \sim \lim_{\substack{\tau \to 0 \\ m \to \infty}} \epsilon^D exp(-\tau d K_2)$$

Using this relation one can estimate $K_2(m,\varepsilon)$ as follows:

$$K_2(m, \varepsilon) = \frac{1}{\tau} \ln \frac{C^m(\varepsilon)}{C^{m+1}(\varepsilon)}$$

Where, correlation integral as per GP algorithm, Ref

$$C(\varepsilon) = \lim_{N \to \infty} \frac{1}{N^2} \times \{\Theta(\varepsilon - \|x_i - x_j\|)\}$$

Though Euclidean norm was used in this case, the choice is arbitrary.

***Estimation of $K_2$ from Recurrence Plots:*** It is clear from Equation 4.2 and 4.3 that

$$C(\varepsilon) = \lim_{N \to \infty} RR$$

Thiel et.al have shown RPs can be employed to calculate $K_2$ and that RPs can also be used to follow the evolution of $K_2$ as a function of ε. The cumulative distribution of diagonal lines $P_\varepsilon^{m,\tau}$ in a RP reconstructed using time delay embedding parameters, m and $\tau$ is given by

$$P_\varepsilon^{m,\tau}(l) = \frac{1}{N^2} \sum_{i,j=1}^{N} \prod_{d=0}^{l-1} \Theta(\varepsilon - \|x_{i+d} - x_{j+d}\|) \qquad 4.11$$

Which can be shown to be related to $K_2$ as follows(Thiel *et al.*, 2004)

$$P_\varepsilon^{m,\tau}(l) \sim \varepsilon^{D_2} exp(-l\tau K_2) \hspace{4cm} 4.12$$

Where $D_2$ is the correlation dimension of the system (Grassberger and Procaccia, 1983b). Therefore, if we represent *ln(Pε (l))* versus *l*, we obtain a straight line with slope $-\tau \widehat{K}_2(\varepsilon)$, where $\widehat{K}_2(\varepsilon)$ is an estimator for $K_2$ .One advantage of using this algorithm is that the result is independent of the embedding parameters used (Thiel *et al.*, 2004).

## 4.3   Results

All methods discussed above were applied to RPM data obtained for seven healthy volunteers. These seven volunteers are henceforth referred to as V1 through V7, were randomly chosen and their breathing was recorded using RPM system for 15 minutes. The first 5 minutes were used as a run-in period to let the dynamical system come to an equilibrium state, and hence this part of the data was not used. The time series data was then embedded in time-delay embedded state space. Recurrence plots were computed with ε such that the Recurrence Rate was equal to 1%. The above detailed parameters, *DET, L_{max}, L_{avg} DIV, ENTR*, and $K_2$ were computed for each breathing time series. The plots were examined qualitatively for presence of UPOs. Time Resolved RP were also examined for automatic detection of pronounced UPOs. A strong variation was found among the seven healthy volunteers, which is presented below.

### 4.3.1  Recurrence Qualitative and Quantitative Analysis

The breathing pattern of V1, V2, and V3 is shown in figures 4-1(a), 4-2(a) and 4-3(a) respectively. The respective reconstructed state-space in 3 dimensions is shown in Figures 4-1(b), 4-2(b) and 4-3(b) respectively. The RP thresholded with ε such that RR is equal to 1% is shown in Figures 4-1(c), 4-2(c) and 4-3(c) respectively. The RP of V2 is dense with many short diagonals and little or no long diagonals. However, the RP of V1 shows longer diagonals

compared to that of V2, sparse initially which eventually grow longer with time. The RP of V3 shows presence of strong long diagonals which are consistent throughout the breathing cycle. Qualitatively, one can also observe dense diagonal lines in V1 and V3 along the main diagonal, which make them very strong candidates of coaching using these dense orbits, i.e. utilizing the UPOs for coaching. However, the RP of V2 has UPOs that are not very strong that exhibit small mean diagonal values, which suggests that V2 might not be a good candidate for coaching. However, chaos control is based on the fact that any chaotic attractor contains an infinite number of these unstable periodic orbits. Chaotic dynamics then consists of a motion where the system state moves in the neighborhood of one of these orbits for a while, then falls close to a different unstable periodic orbit where it remains for a limited time, and so forth. This results in a complicated and unpredictable wandering of the trajectory over longer periods of time. Hence, if one waits for a sufficiently long time period, one will be able to identify UPOs for a given nonlinear dynamical system. This may however be impractical in Radiation Therapy applications.

Table 4-1 shows the RQA parameters calculated for the breathing patterns collected for the 7 volunteers over the entire duration of 600 sec. Looking at the data in table 4-1 one observes that the mean diagonal lengths are ordered as follows V3>V1>V2. Likewise, determinism and max diagonal lengths follow this ordering V3>V1>V2.

## 4.3.2 Time Resolved RQA for automatic UPO detection

For all RPs, time resolved RPs were also calculated. The RR in each overlapping segment was calculated and plotted over time. This is shown in Figure 4-4(a), 4-5(a) and 4-6(a) for V1, V2, and V3. The maximum two or three peak *RR* values and their respective time of occurrence were used to go back into the RP to check for the presence of UPOs. This method successfully detected the strongest UPOs that can be detected in the RP using visual inspection. The RP over

these time windows are zoomed for better visualization and are shown in Figure 4-4(c)-(d), 4-5(c)-(e),4-6(c)-(e) respectively for V1,V2,V3. RQA analysis on the UPOs shows long diagonals with larger $L_{avg}$ values. This shows that if one could coach patients to comfortably reenter their UPOs, larger prediction horizon could be achieved.



**Figure 4-2:** 1-D time series and the embedded time space in 3D($\tau$ =1.06 sec) for Volunteer 1 is shown in (a) and (b) respectively. Recurrence plot of the time series shown in (a) is displayed in (c) with Recurrence Rate equal to 1.0.
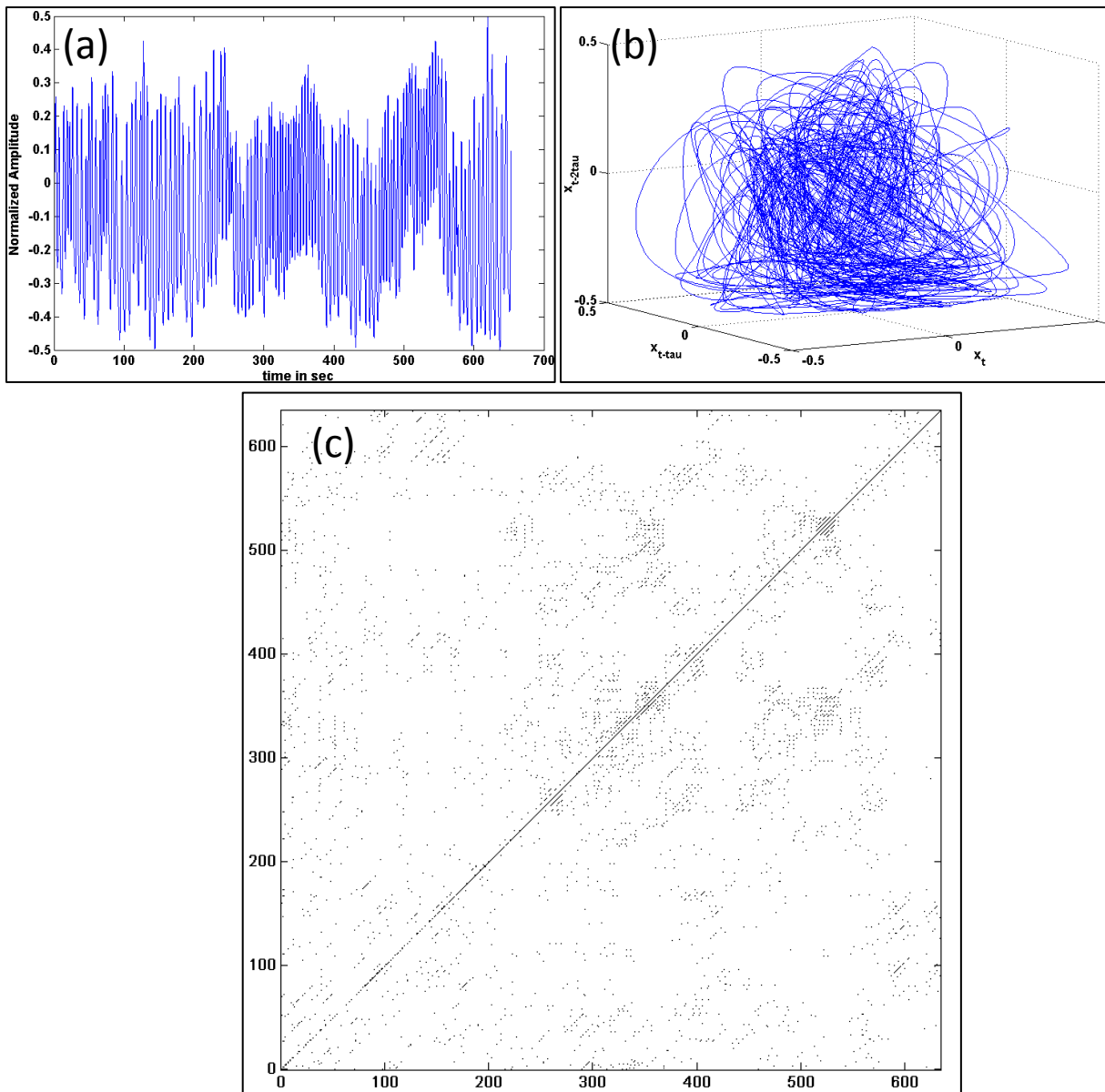
**Figure 4-3:** 1-D time series and the embedded time space in 3D($\tau$ =4.5 sec) for Volunteer 2 is shown in (a) and (b) respectively. Recurrence plot of the time series shown in (a) is displayed in (c) with Recurrence Rate equal to 1.0

### 4.3.3 Prediction Plots

For use of RPs as a tool for prediction assessment, the time series was first undersampled by a factor of 6, thus yielding a time series with a sampling frequency of 5 Hz. With the advent of

newer technologies the above mentioned methods can be directly implemented on *1D* tumor trajectories. This sparcified data was then divided into two parts, the first 300 seconds were used as a training set. The results of which were then used for prediction of the next 300 seconds, the length of training set was updated going forward with time. RQA parameters were computed for the second half of the breathing series data (300-600 seconds) of the RPs calculated from the embedded under sampled 1D time series. NRMSE for all volunteers was plotted as a function of the following RQA parameters: Determinism, $L_{avg}$, and Entropy. A linear model shows a good fit for the plotted data points, NRMSE points against Determinism with a coefficient of determination ($R^2$) of 0.95

A power model fitted to the data points, NRMSE vs $L_{avg}$ shows a good agreement with $R^2$ of 0.98 which leads one to infer that $L_{avg}$ is a good indicator for predictability. NRMSE plotted against Entropy shows a linear fit with a $R^2$ value of 0.82.

### 4.3.4  Calculation of correlation entropy K2

The algorithm to calculate $K_2$ from RPs is illustrated in figure 4-9. These quantities vary with time and hence, the use of invariant quantities such as $K_2$ with average diagonals can be used for assessment of prediction horizon. Figure 4-9(a) shows the RP for *V3* calculated with $\varepsilon$ such that RR=1%. Figure 4-9(b) shows the cumulative probability of diagonal lines of at least length *l* or greater plotted against *l* for different $\varepsilon$ values. The slope of the lines for *l*>30 gives an estimate of correlation entropy. The local slope of the plot in (b) is shown in (c). For a specific range of *l* values, all the curves run parallel to each other and the local slope converges to a value, which divided by time interval $\tau$ is $K_2$. This is plotted in (d) against *RR* (calculated using the different values of ε). For *V3,* it can be seen that the $K_2$ is the value of the plateau region in 4-9(d), and is approximately equal to 0.052.
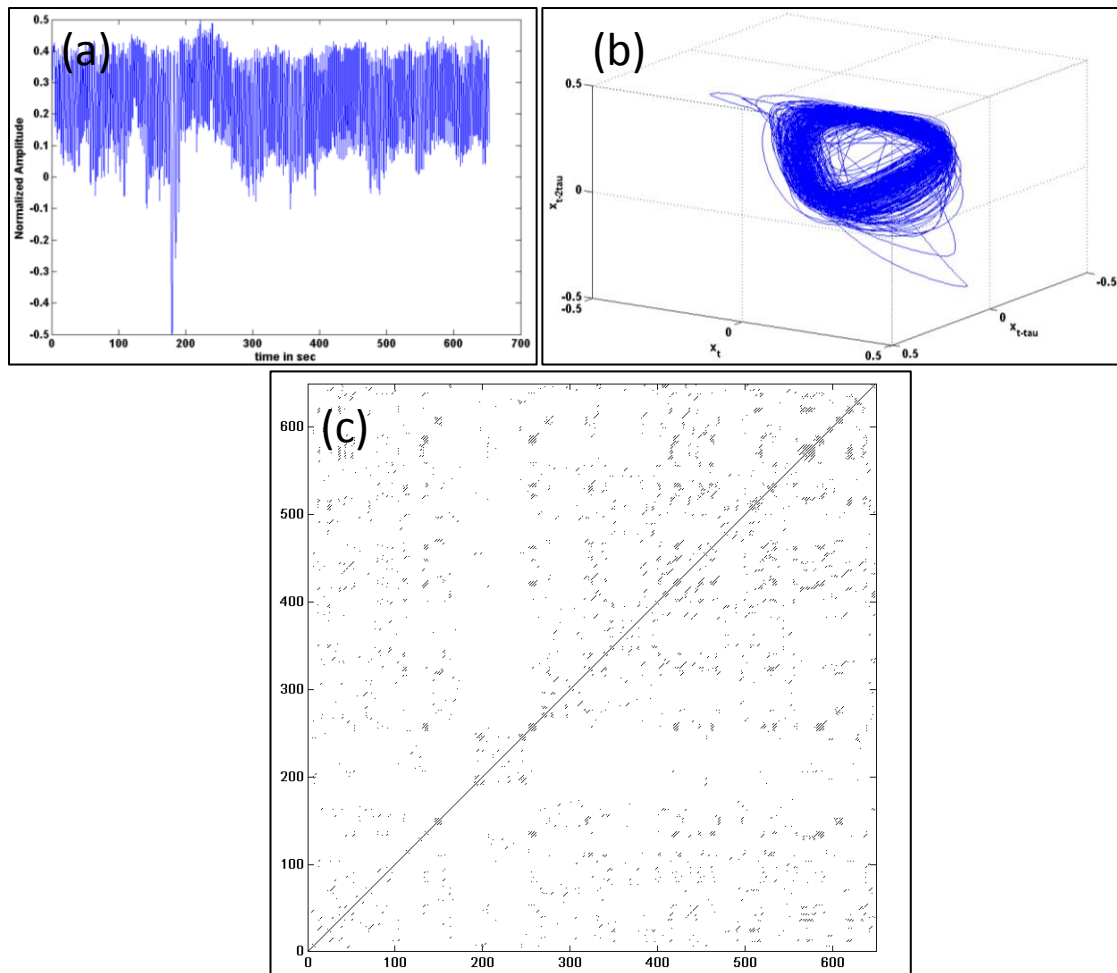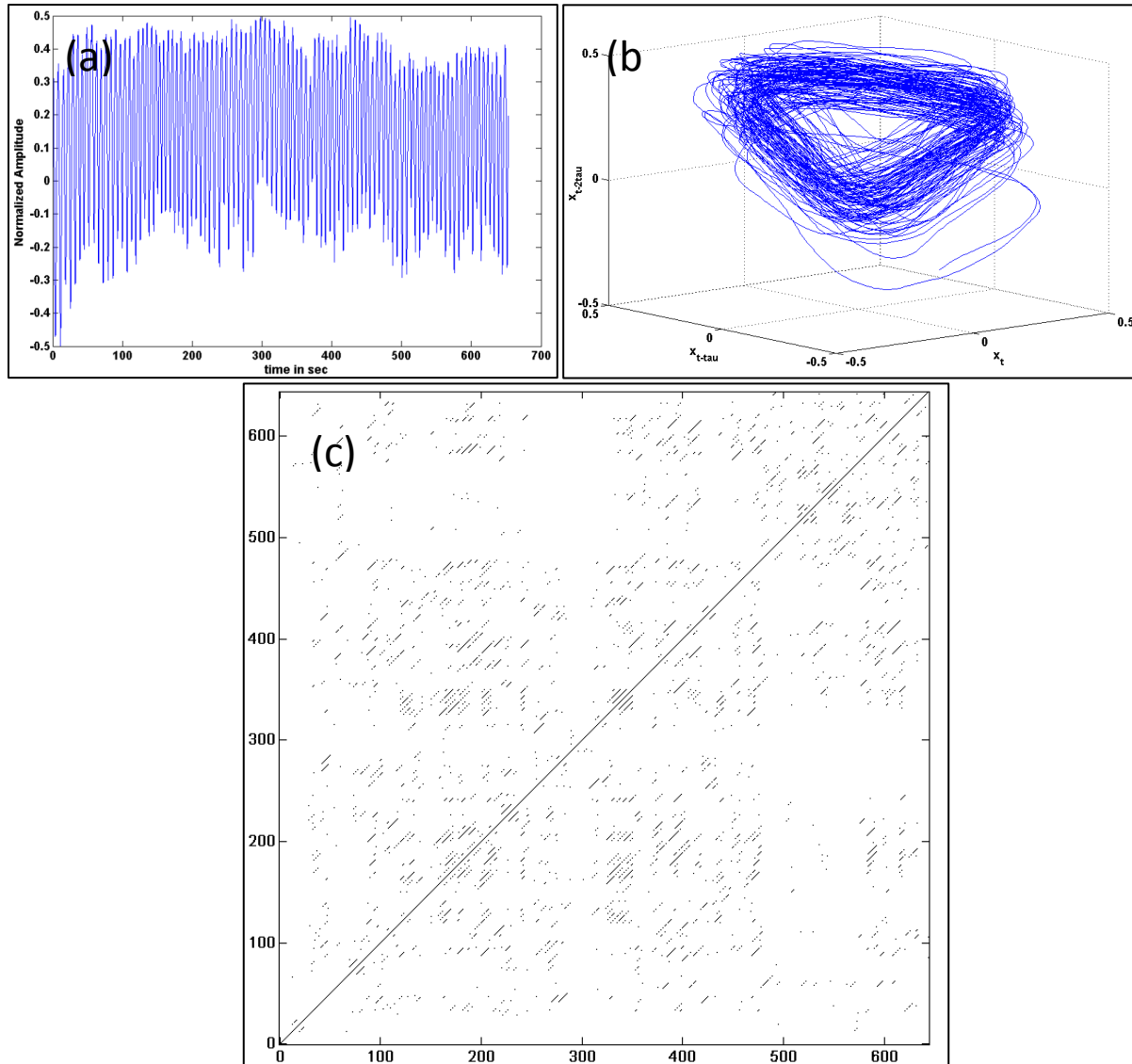
**Figure 4-4:** 1-D time series and the embedded time space in 3D ($\tau$ =2.1 sec) for Volunteer 3 is shown in (a) and (b) respectively. Recurrence plot of the time series shown in (a) is displayed in (c) with Recurrence Rate equal to 1.0.
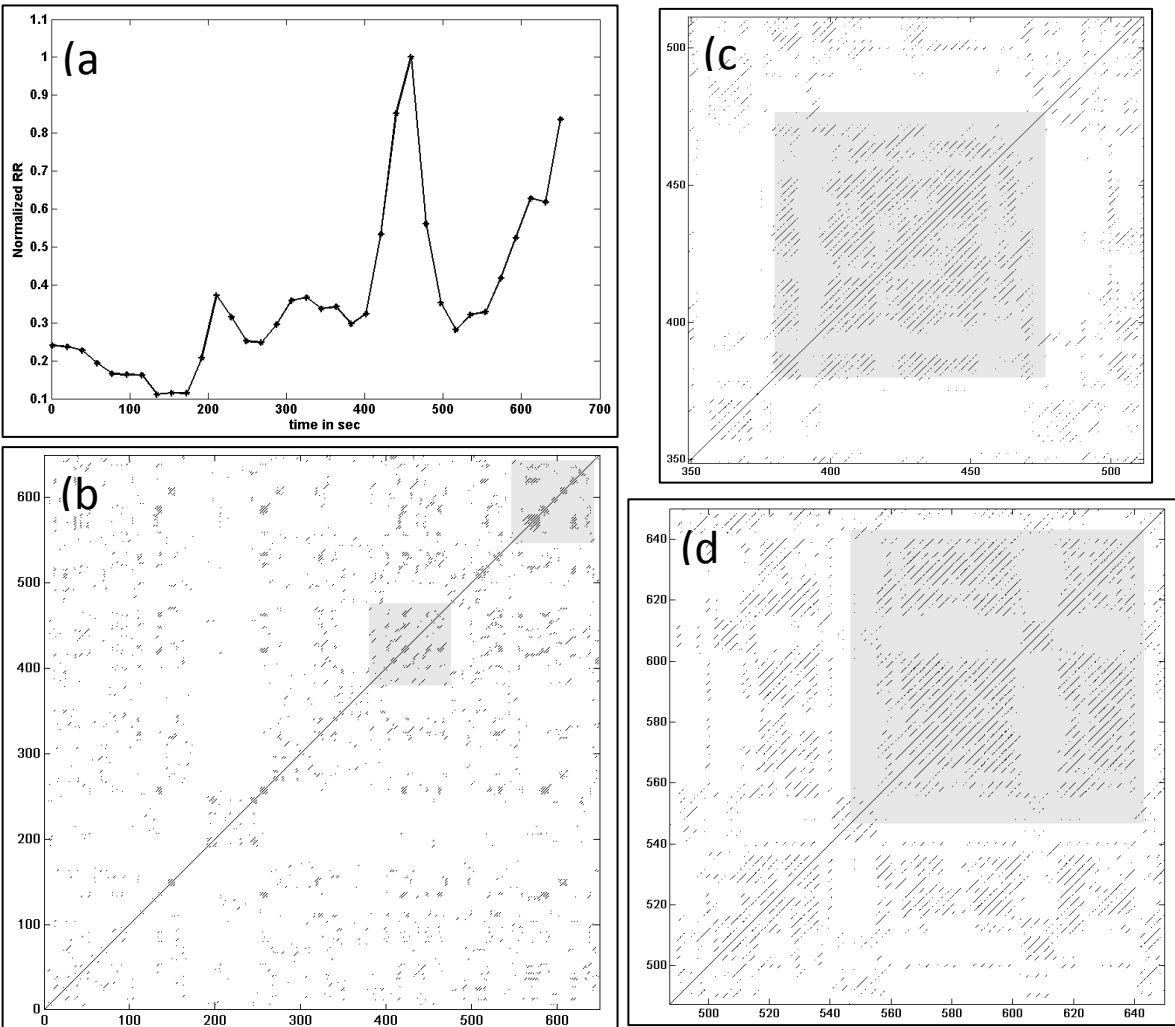
**Figure 4-5:** Normalized Recurrence Rate plotted as a function of epochs using Time Resolved RQA is shown in (a) for Volunteer 1. Based on the location of prominent peaks of RR , automatic detection of UPO in global RP is shown in(b). (c) and (d) are zoomed in views of the two prominent UPOs shown as greyed regions in (b).
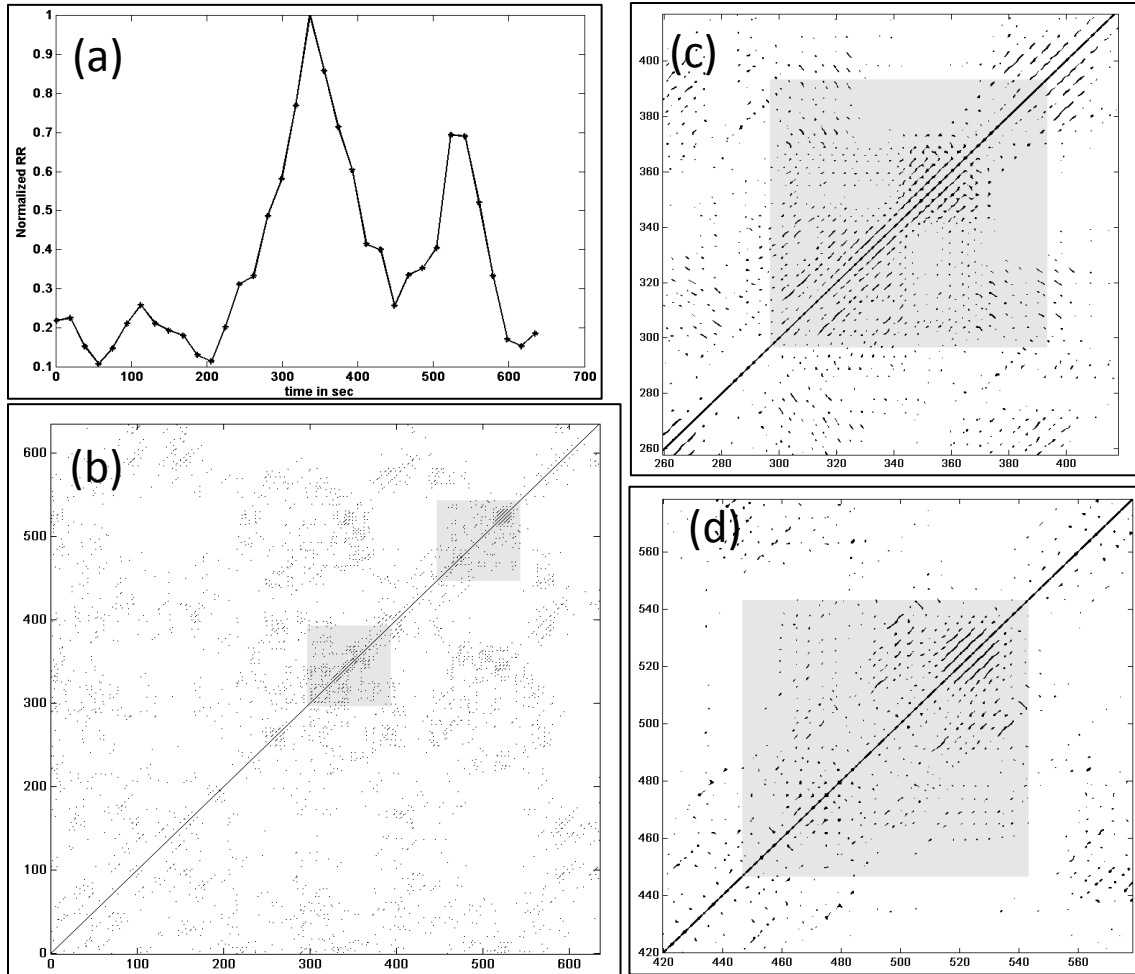
**Figure 4-6:** Normalized Recurrence Rate plotted as a function of epochs using Time Resolved RQA is shown in (a) for Volunteer 2. Based on the location of prominent peaks of RR , automatic detection of UPO in global RP is shown in(b). (c) and (d) are zoomed in views of the two prominent UPOs shown as greyed regions in (b).
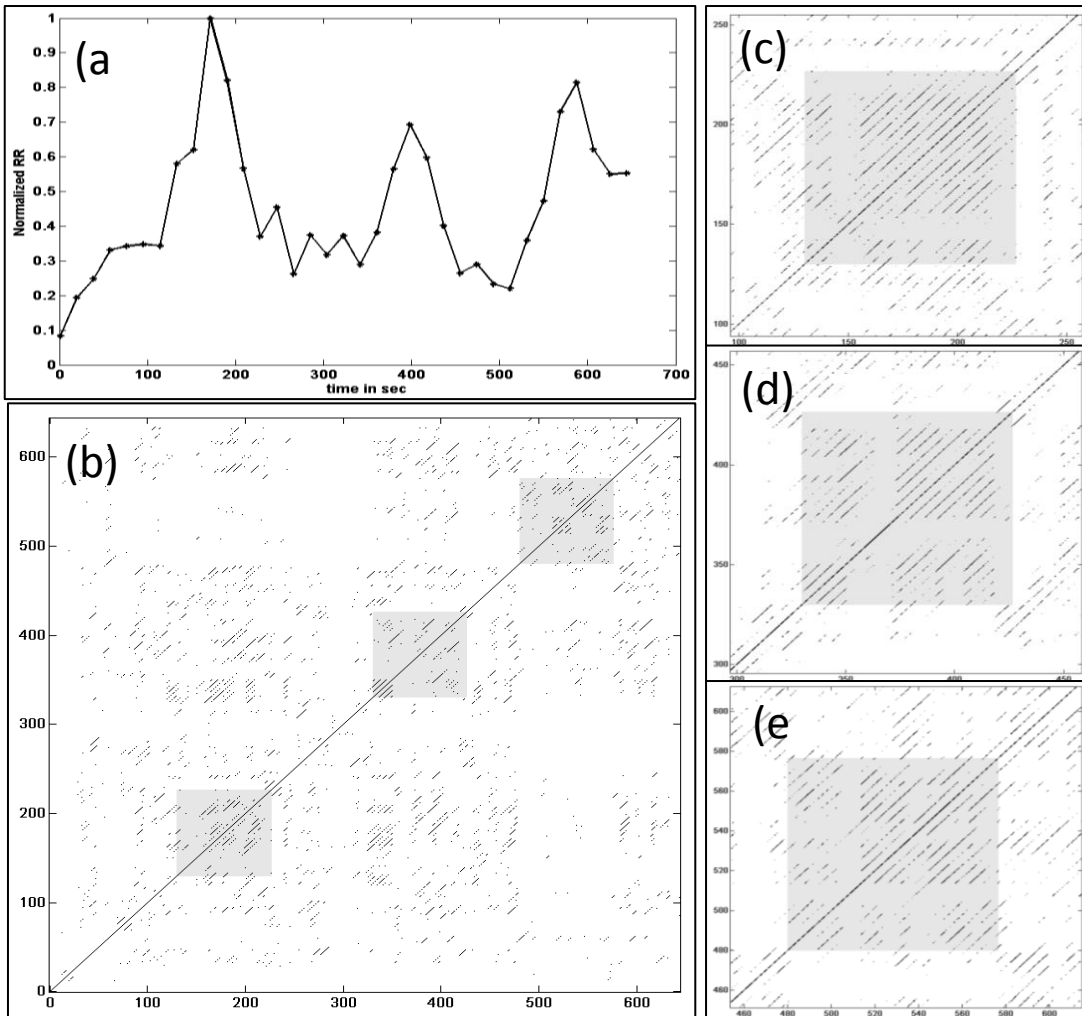
**Figure 4-7:** Normalized Recurrence Rate plotted as a function of epochs using Time Resolved RQA is shown in (a) for Volunteer 3. Based on the location of prominent peaks of RR , automatic detection of UPO in global RP is shown in(b). (c) and (d) are zoomed in views of the two prominent UPOs shown as greyed regions in (b).
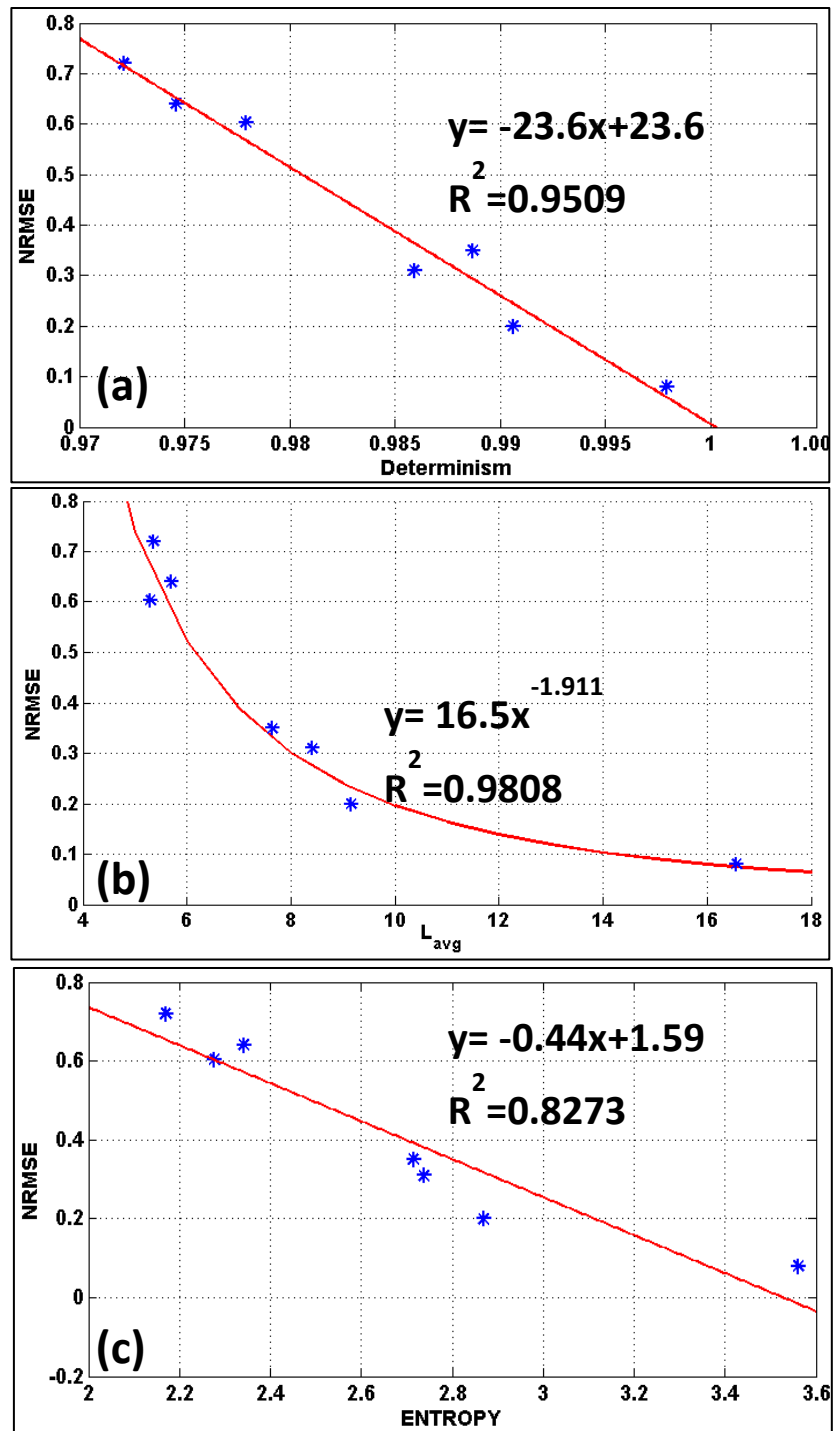
**Figure 4-8:** Plot of NRMSE plotted against determinism calculated using RP is shown in (a). A linear fitting line shows a correlation coefficient of 0.95. Plot of NRMSE vs average length of

diagonals shows a power relation with a correlation coefficient of 0.98. (c) shows a linear fitted relationship between NRMSE and Entropy
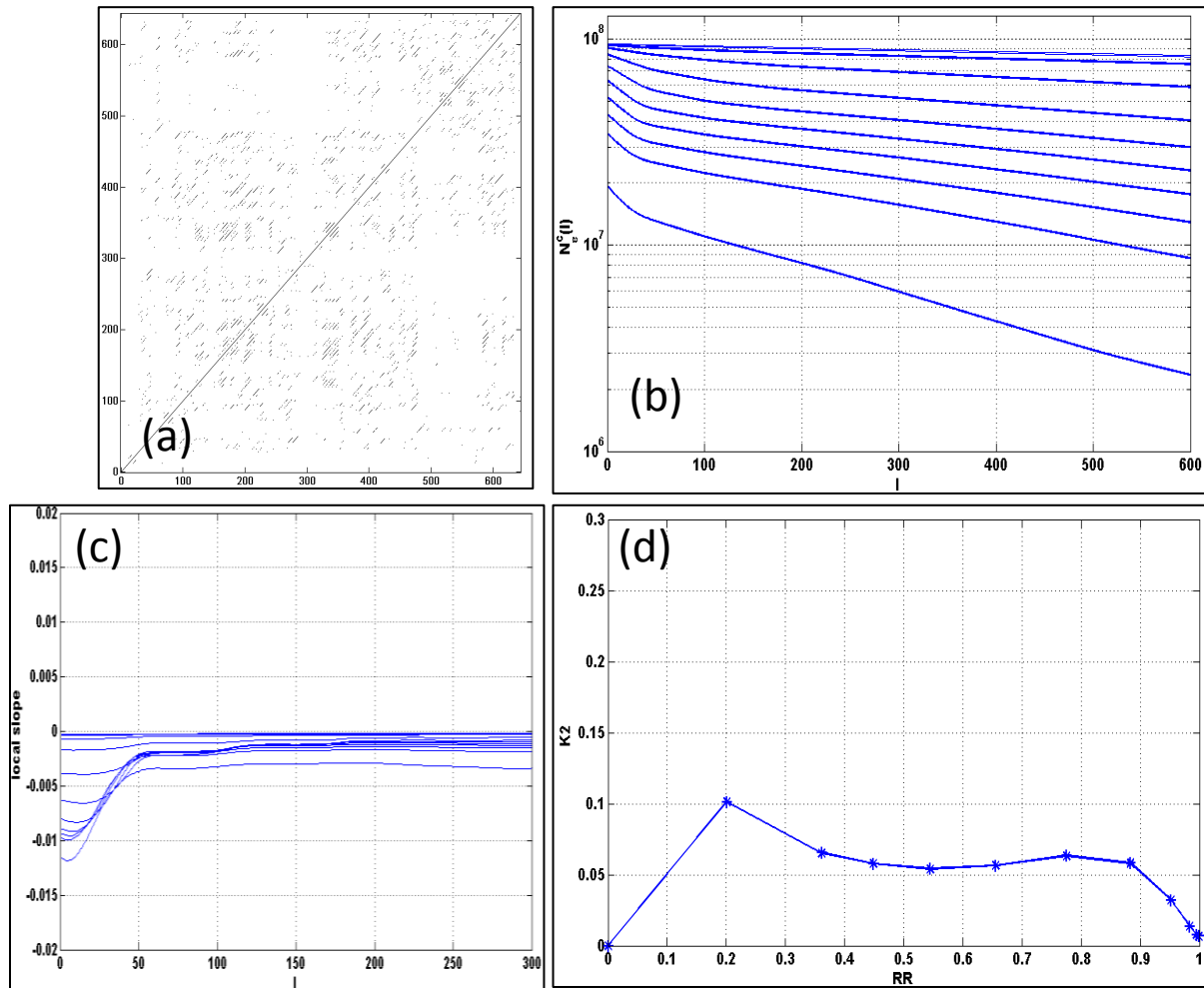


**Figure 4-9:** Calculation of K2 for volunteers 7 is shown in the above figure. (a) shows the global RP for Volunteer 3. The plot of cumulative number of diagonal lengths as a function of l for different $\varepsilon$ is shown in (b). Local slope of each of the curves shown in (b) against l is shown in (c). Correlation entropy $K_2$ as a function of RR is shown in (d).

| Volunteer | DET | LAVG | DIV | LMAX | ENTR | K2 |
|-----------|------|-------|--------|------|--------|-------|
| 1 | 0.9887 | 19.5 | 0.0021 | 479 | 3.7135 | 0.12 |
| 2 | 0.9852 | 12.26 | 0.0056 | 177 | 3.1892 | 0.15 |
| 3 | 0.9942 | 24.75 | 0.0011 | 945 | 3.99 | 0.052 |
| 4 | 0.9873 | 16.16 | 0.0017 | 595 | 3.4892 | 0.065 |
| 5 | 0.9782 | 13.55 | 0.0015 | 650 | 3.2815 | 0.1 |
| 6 | 0.993 | 20.1 | 0.0025 | 408 | 3.7706 | 0.105 |

**Table 4-1:** RQA Data for all volunteers calculated from over the entire length of data collected(~600 sec)

## 4.4   Discussion and Conclusion

We have introduced quantitative analysis tools that can be used as a guidance to select appropriate 4D treatment strategy for lung cancer patients. We have shown that the RQA parameters found using Recurrence plots can be used as a good assessment for predictability and complexity of the patient's breathing pattern. $K_2$ values calculated are invariant quantities and give an approximation of how chaotic the signal under consideration is. Higher the value, more complex is the breathing. We have also shown the Time Resolved RQAs can be used for automatic detection of UPOs that can be used for coaching patients. Volunteers 3 and 7 RP showed presence of long diagonals with no trending, which shows that these patients are suitable candidates for prediction alone without coaching/breathing control. However, volunteers whose Lavg peaks vary significantly along time-resolved RQAs (V1, V4), would be good candidates for prediction provided control mechanisms are used for the patients. For volunteers with low average diagonal lengths, and absence of strong UPOs (V2, V5), it would be best to obtain an ITV for tumor motion assessment.

With the advent of newer tumor tracking technologies such as the Calypso tracking system (Calypso, Seattle, Washington), RealEyeTM Motion (Navotek Medical Ltd, Yokneam, Israel), or real time MR Radiotherapy systems like the one being developed by Viewray (Viewray Inc.,

Cleveland, OH) with which it will be possible to acquire real-time MR images at a frame rate of 4 images/sec coupled with fast treatment delivery methods such as VMAT, tumor tracking can become a reality. Using the methods introduce in this work will allow one to identify patients who will benefit from these 4D treatment strategies by employing coaching to allow them to reenter strong UPOs and hence leading to longer prediction horizons, and those that are better served employing ITV based treatments.

Future work will include assessment of patient breathing patterns including non-stationary signals. Non-stationarity can introduce large prediction errors. Qualitatively, fading in RPs indicates trending or non-stationarity which can be quantified and related to prediction errors. Quantitative Recurrence Analysis can be a very powerful mathematical tool that can be used for segregating patients into different 4D treatment strategies, based on their variability of breathing.

## 4.5   Reference

Bradley E and Mantilla R 2002 Recurrence plots and unstable periodic orbits *Chaos: An Interdisciplinary Journal of Nonlinear Science* **12** 596

Eckmann J P, Kamphorst S O and Ruelle D 1987 {Recurrence plots of dynamical systems} *EPL (Europhys. Lett.)* **4** 973-7

Gomez D R and Chang J Y 2011 Adaptive Radiation for Lung Cancer *Journal of Oncology* **2011** Grassberger P and Procaccia I 1983a Characterization of Strange Attractors *Physical Review Letters* **50** 346

Grassberger P and Procaccia I 1983b Measuring the strangeness of strange attractors *Physica D: Nonlinear Phenomena* **9** 189-208

Kantz H and Schreiber T 2004 *Nonlinear time series analysis*: Cambridge Univ Pr)

Kugiumtzis D 2002 State space local linear prediction *Modelling and Forecasting Financial Data, Techniques of Nonlinear Dynamics*  95–113

Marwan N, Carmen Romano M, Thiel M and Kurths J 2007 Recurrence plots for the analysis of complex systems *Physics Reports* **438** 237-329

Mechalakos J, Yorke E, Mageras G S, Hertanto A, Jackson A, Obcemea C, Rosenzweig K and Clifton Ling C 2004 Dosimetric effect of respiratory motion in external beam radiotherapy of the lung *Radiotherapy and Oncology* **71** 191-200

Nuyttens J J, Prévost J-B, Praag J, Hoogeman M, Van Klaveren R J, Levendag P C and Pattynama P M T 2006 Lung tumor tracking during stereotactic radiotherapy treatment with the CyberKnife: Marker placement and early results *Acta Oncologica* **45** 961-5

Sawant A, Smith R L, Venkat R B, Santanam L, Cho B, Poulsen P, Cattell H, Newell L J, Parikh P and Keall P J 2009 Toward Submillimeter Accuracy in the Management of Intrafraction Motion: The Integration of Real-Time Internal Position Monitoring and Multileaf Collimator Target Tracking *International Journal of Radiation Oncology*Biology*Physics* **74** 575-82

Seppenwoolde Y, Berbeco R I, Nishioka S, Shirato H, Heijmen B, Brigham, Hospital W s, Harvard Medical School B, Massachusetts 02115, Department of Radiation Oncology N E J S H, Sapporo, Department of Radiation Medicine H U S o M, Sapporo and Department of Radiation Oncology D o M P, ErasmusMC, Rotterdam] 2007 Accuracy of tumor motion compensation algorithm from a robotic respiratory tracking system: A simulation study *Journal Name: Medical Physics; Journal Volume: 34; Journal Issue: 7; Other Information: DOI: 10.1118/1.2739811; (c) 2007 American Association of Physicists in Medicine; Country of input: International Atomic Energy Agency (IAEA)* Medium: X; Size: page(s) 2774-84

Shirato H, Shimizu S, Kitamura K, Nishioka T, Kagei K, Hashimoto S, Aoyama H, Kunieda T, Shinohara N and Dosaka-Akita H 2000 Four-dimensional treatment planning and fluoroscopic real-time tumor tracking radiotherapy for moving tumor* 1 *International Journal of Radiation Oncology* Biology* Physics* **48** 435-42

Tewatia D K, Tolakanahalli R P, Paliwal B R and Tome W A 2011 Time series analyses of breathing patterns of lung cancer patients using nonlinear dynamical system theory *Phys Med Biol* **56** 2161-81

Thiel M, Romano M C, Read P L and Kurths J 2004 Estimation of dynamical invariants without embedding by recurrence plots *Chaos (Woodbury, N.Y.)* **14** 234-43

Zbilut J, Giuliani A and Webber C 1998 Recurrence quantification analysis and principal components in the detection of short complex signals *Physics Letters A* **237** 131-5

# Chapter 5. Novel methodology for chaos control in breathing patterns of lung cancer patients

## 5.1 Introduction

Lung tumors can show significant respiration-induced motion (Liu *et al.*, 2007; van Sörnsen de Koste *et al.*, 2003), which in turn confounds radiotherapy planning and delivery (Keall *et al.*, 2006). Individualized assessment of tumor mobility is recommended for treatment planning in lung cancer (Senan *et al.*, 2004). American Association of Physicists in Medicine (AAPM) Task Group 76 recommended that motion management should be considered for any tumors showing more than 5 mm of motion (Keall *et al.*, 2006), Variation caused by irregular breathing adversely affects the ability of the respiration monitor system to accurately calculate phases, whereas changes in respiration amplitude result in inconsistent amounts of anatomic motion in different slices of an image set (Mutaf *et al.*, 2007). For 4DCT imaging and gated radiation therapy, breathing control has been addressed by many in the past using video coaching and/or audio coaching. Several authors have concluded that audio coaching could increase the amplitude of breathing, thus affecting the tumor position displacement (Neicu *et al.*, 2006; Persson *et al.*, 2008; Haasbeek *et al.*, 2008). With the technological advances, effective compensation of tumor motion can be achieved by tracking and targeting the tumor in realtime. Delivery using synchronization methodologies requires knowledge of real-time tumor position to overcome or account for system latency. Predicting respiratory motion in real-time is challenging, due to the inherent chaotic nature of breathing patterns, i.e. sensitive dependence on initial conditions (Tewatia *et al.*, 2011). However, short time prediction of the chaotic signals can still be achieved

by using state-space prediction methodologies (Tolakanahalli, 2012). The prediction horizon regardless of the prediction methodologies can be increased if the breathing pattern of the patient can be regularized for a limited amount of time. Limited success has been achieved by many in the past using audio coaching. However, coaching methods tailored for patient specific breathing has not been explored in radiation therapy before. Here, we intend to use control mechanisms well explored in chaos theory to simulate and build a theoretical model for breathing control

We discuss the methods employed and the in-house system built for acquiring, locating the UPO and biofeedback methods in some detail in section 5-2. We also introduce theoretical underpinning of chaos control mechanism in Section 5-2. In section 5-3 we report on the results we have obtained using a sample volunteer data. In section 5-4 we discuss the implications of our findings and discuss in detail future directions this work could engender.

## 5.2   Methods and materials

### 5.2.1  Overview of Chaos Control

This method of control is based on the following concepts: Stability, feedback and flexibility. The idea behind the concept of flexibility is that it is not necessary to stress the system and drive it brutally to the desired operation point. In contrast, it is more efficient to slightly perturb the system and let the system fluctuate and settle into the desired state for a short amount of time. Sensitive dependence on initial conditions make it very hard to make long time predictions, but this property can be exploited for changing the trajectory's future by slightly perturbing the system. Besides, a carefully chosen set of small perturbations applied continuously can rapidly drive the system to a desired final state- and this methodology is called targeting. Smale (Smale, 1966), by using symbolic dynamics, showed that this invariant set has a dense orbit, exhibits the

sensitivity to initial condition property, and embedded in it there is a countable infinity set of unstable periodic orbits(UPO) of arbitrary high periods. Let us consider a system in which a non-attracting chaotic saddle coexists in the phase space with others nonchaotic attractors. As there are other attractors in the phase space, all initial conditions, except for a set of measure zero made up of the chaotic saddle and its stable manifold, generate trajectories that asymptote to one of the attractors. Trajectories starting from random initial conditions may wander near the chaotic saddle for a finite time before settling down into one of the attractors. During the time interval in which a trajectory suffers the influence of the chaotic saddle, it behaves as a chaotic trajectory. Furthermore, the closer the initial condition of a trajectory to the stable manifold, longer the trajectory stays near the chaotic saddle, exhibiting a chaotic-like behavior (Scholl and Schuster, 2008).

If the system such as the respiratory dynamical system has a UPO which is suitable as an operating condition, stabilization of this orbit may be an option that should be explored. The closer a chaotic trajectory approaches a periodic orbit; the longer the trajectory tends to remain in its neighborhood. Chaos control can help re-establish at least a regular periodic output at higher rate, with judiciously applied minimal perturbations. For a systematic approach of the control problem, the first step is to find the location of the unstable periodic orbits from the experimental time series based on patients breathing pattern. A change of the operating condition can be accomplished simply by waiting until the uncontrolled system comes sufficiently close to the desired orbit. When the system moves towards this stable orbit, a tiny perturbation will suffice to push it on to the orbit (Baker, 1995). Estimating the parameter and the correct perturbation is the key to chaos control. Appropriate perturbation of the trajectory directly using the information about the tangent space structure in the neighborhood of the target orbit, allows one to push the

trajectory onto the stable manifold of the attractor. Control then consists of changing the parameter slightly to move the trajectory towards the opposite side of the stable orbit. The trajectory feels the repulsion due to the instability towards the opposite directions and will therefore be pushed towards the original position of the stable manifold.

## 5.2.2 OGY Method in Chaos Control

We review a scenario of a chaotic dynamical system whose attractor is a three-dimensional state space (Ott *et al.*, 1990). A Poincaré section can be introduced transversal to the chaotic flow so that the system dynamics on this Poincaré section can be described by a two-dimensional invertible map as

$$x_{n+1} = \mathcal{F}(x_n, p) \hspace{4cm} 5.1$$

Where $x_n \in \mathbb{R}^2$, $\mathcal{F}$ is a smooth function of its variables, and $p \in \mathbb{R}$ is an externally accessible control parameter. Following the idea of using small perturbations to control the system, parameter allowed variations must be small,

$$|p - \bar{p}| < \delta \hspace{4cm} 5.2$$

where $\bar{p}$ is the nominal parameter value, and $\delta \ll 1$ defines the allowable range of parameter variation. We wish to program the parameter p so that a chaotic trajectory is stabilized when it enters in a neighborhood of the target periodic orbit.

Let $x_F(\bar{p})$ be one of the fixed points of the map at the nominal parameter value $\bar{p}$ that we wish to stabilize. The location of the fixed point in the phase space depends on the control parameter p. Upon application of small perturbation $\Delta p$, we have $p = \bar{p} + \Delta p$. Since $\Delta p$ is small, we expect $x_F(p)$ to be close to $x_F(p)$. We write

$$x_F(p) = x_F(\bar{p}) + g\Delta p \hspace{6cm} 5.3$$

where the vector g is given by

$$g \equiv \left.\frac{\partial x_F}{\partial p}\right|_{p=\bar{p}} \approx \frac{x_F(p) - x_F(\bar{p})}{\Delta p} \hspace{5cm} 5.4$$

The system dynamics of any smooth nonlinear system is approximately linear in a small $\varepsilon$ neighborhood of a fixed point. Thus, near we can use the linear approximation for the map:

$$[x_{n+1} - x_F(p)] \approx M[x_F(p)].[x_n - x_F(p)] \hspace{4cm} 5.5$$

where $M[x_F(p)]$ is the 2 x 2 Jacobian matrix of the map $\mathcal{F}(x,p)$ evaluated at the fixed point $x_F(p)$, which is defined as follows:

$$M[x_F(p)] = \left.\frac{\partial \mathcal{F}}{\partial x}\right|_{x_F(p)} \approx M[x_F(\bar{p})] + \left.\frac{\partial M}{\partial p}\right|_{p=\bar{p}} \Delta p \hspace{3cm} 5.6$$

Note that $\Delta p \sim \varepsilon$ and $|[x_n - x_F(p)]| \sim \varepsilon$, where $\varepsilon$ is the size of the small neighborhood in which the linear approximation is valid. Substituting (5.4) and (5.6) into Equation (5.5), and keeping only terms which are first order in $\varepsilon$, we obtain

$$x_{n+1} - x_F(p) \approx g\Delta p + M[x_F(\bar{p})].[x_n - x_F(\bar{p}) - g\Delta p] \hspace{3cm} 5.7$$

In Equation (5.7), the Jacobian matrix $M$ is evaluated at the fixed point $x_F(\bar{p})$ of the unperturbed system, which is the one to be stabilized. Since $x_F(\bar{p})$ is embedded in the chaotic attractor, it is unstable and it has one stable and one unstable direction (Garfinkel *et al.*, 1992). Let $e_s$ and $e_u$ be the stable and unstable unit eigenvectors at $x_F(\bar{p})$, respectively, and let $f_s$ and $f_u$ be two unit vectors that satisfy $f_s.e_s = f_u.e_u = 1$ and $f_s.e_s = f_u.e_u = 0$, which are the relations by which the vectors $f_s$ and $f_u$ can be determined from the eigenvectors $e_s$ and $e_u$. The vectors $f_s$ and $f_u$ are contravariant basis vectors associated with the eigenspace $e_s$ and $e_u$.

The Jacobian matrix $[x_F(\bar{p})]$ , can then be written as:

$$M[x_F(\bar{p})] = \lambda_u f_u e_u + \lambda_s f_s . e_s \qquad \text{5.8}$$

where $\lambda$s and $\lambda$u are the stable and unstable eigenvalues in the eigendirections e$_s$ and e$_u$ respectively. When the trajectory point x$_n$ falls into small $\varepsilon$ - neighborhood of the desired fixed point $x_F(\bar{p})$ so that Eq. 5.5 applies, a small parameter perturbation $\Delta p_n$ is applied at time n to make the fixed point shift slightly so that at the next iteration (n+1), x$_{n+1}$ falls on the stable direction of $x_F(\bar{p})$ . Thus, we choose the parameter control $\Delta p_n$ such that

$$f_u[x_{n+1} - x_F(\bar{p})] = 0 \qquad \text{5.9}$$

If xn! 1 falls on the stable direction of $x_F(\bar{p})$ , we can then set the control perturbation to zero, and the trajectory for subsequent time will approach the fixed point at the geometrical rate $\lambda$s. Thus for sufficiently small $x_n - x_F(\bar{p})$ , we can substitute Equation 5.7 into Equation 5.9 to obtain $\Delta p_n = c_n$:

$$c_n = \frac{\lambda_u f_u . [x_n - x_F(\bar{p})]}{(\lambda_u - 1) f_u g} \equiv C[x_n - x_F(\bar{p})] \qquad \text{5.10}$$

We assume in the above that the generic condition $g. f_u \neq 0$ is satisfied so that $c_n \sim [x_n - x_F(\bar{p})]$ which is small. The considerations above apply only to a local small neighborhood of $x_F(\bar{p})$. Globally, we can specify the parameter perturbation $\Delta p_n = 0$ if $|c_n|$ is too large, since the range of the parameter perturbation is limited by Equation 5.2. Thus, practically, we can take $\Delta p_n$ to be given by

$$\Delta p_n = \begin{cases} c_n & if \ |c_n| < \delta \\ 0 & if \ |c_n| \geq \delta \end{cases} \qquad \text{5.11}$$

where in the definition of $c_n$ in Eq. (5.10), it is not necessary to restrict the quantity $x_n - x_F(\bar{p})$ to be small. This method can be extended to higher dimensional systems.

The inherent exponential sensitivity of chaotic time evolution to perturbations can be intelligently exploited to direct the dynamics of the system to some desired state using a carefully chosen sequence of small perturbations to some system parameter. This approach, which is of fundamental interest for the control system, is called targeting (Shinbrot *et al.*, 1990). The targeting idea came about as a way to get around an excessive transient time associated with the use of the OGY method of chaos control to higher dimensional systems. The classical method is used first, just to drive the trajectory to the neighborhood of the UPO. From this point on, the OGY strategy is then applied so that the system is kept stabilized by using small perturbations.

### 5.2.3  Data acquisition and Processing

Respiration Monitor Belt by Vernier (Oregon, USA) was wrapped around the chest snugly , with the Velcro straps pressed together at the back. The belt was positioned such that the airbladder is resting over the base of the ribcage as shown in Figure (5-2).  The pressure of the airbladder is comfortably set according to the volunteers requirement while making sure that the variation in pressure with inhalation and exhalation is about 2-3 kPa. The pressure is measured using a Gas Pressure Sensor (Vernier ,Oregon, USA), which has a membrane that flexes as the pressure changes. The pressure sensor is connected to a SensorDAQ interface providing connectivity between the pressure sensor and a Windows computer running a Labview software via a USB interface. Labview Code can be logically split into 2 parts. The first section of the code is acquisition of breathing cycle for analysis and reconstruction of state-space, detection of UPOs and a finding a suitable target UPO for coaching. This flow with screenshots of the

Labview program is shown in Figure 5-3. The time series corresponding to the target UPO is then chosen and automatic peak detection is performed. The time series signal between the first and the last peak is appended to form a continuous coaching signal which is then fed to the second section of the LabView code.

This section monitors the current breathing pattern of the patient and provides a guide based on the target UPO. The resulting waveform was then analyzed using Recurrence Quantification Analysis to analyze the effect of guiding.

## 5.2.4 Proposed Real Time Targeting Algorithm

In order to systematically implement the control strategy, it is first necessary to identify patients who have strong multiple UPOs that can be used for targeting and control. This part was introduced and explained in Chapter 3.

The following algorithm is proposed for realtime targeting of the

i.    Acquire patients breathing for about 5 minutes and locate UPOs. This is done by first finding the right delay based on mutual information method and finding correct embedding dimension. Based on the Recurrence rate and average diagonal length using Time-Resolved RQAs , two to three UPOs are located.

ii.   Series of intercycle breathing period (IBP) is embedded into two-dimensional space by plotting current IBP $x_n$ against its previous IBP ,$x_{n-1}$.

iii.  The state-space is searched for localization of the target UPO as described in the previous section, viz. Time-Resolved Recurrence Plot.

iv.   Locate $X_t$, the center of target breathing period, based on UPOs. This should correspond to a fixed point on the return map, i.e a single point on the diagonal of the return map. Such a point will have associated with it stable and unstable direction,

along which the trajectory approaches and diverges from the fixed point. Stable Manifold Placement (SMP) as described by Slutzky and Mogul (Slutzky and Mogul, 2000) is used for locating stable and unstable manifolds , since this technique requires little or no assumptions about system parameters. In order to do this, track the location and movement of IBPs with respect to the fixed point $X_t$. The previous state leading to the fixed point, probably lies close to the stable direction which leads the system to the fixed point. The next state leading the system away from the fixed point represents the unstable direction.

v. Once, this is achieved, the next step is to start collecting data and plotting the points real-time on the return map. Let $z_n=(x_{n-1},x_n)$ be the current state vector and $z^*=(x^*,x^*)$ be the fixed point located using Step ii. The next step is to video coach the patient to follow a breathing pattern with breathing periods such that in increments, the patients IBP comes closer to the stable manifold. It is then important to continuously vary the IBP of the UPO chosen such that the system is just slightly perturbed to stay within a small neighborhood of the UPO. In summary, based on realtime IBP, provide feedback to put the patient on stable manifold and watch the system converge to $X_t$. The control signal to change the period of the orbits will be provided, whose amplitude/period will be proportional to the difference between the current state point and the fixed point.

In this chapter, data sample from one volunteer was acquired for 300 seconds. This was analyzed for UPOs, and using automatic peak detection algorithm, a coaching signal was generated as a guide for the patient to follow. The volunteer was instructed to follow the guiding signal and the resulting waveform was analyzed for reproducibility. Retrospectively, the return

map based on the initial 300 seconds of data was used to construct a return map, and a fixed point based on the UPO was computed. The stable and unstable directions manifold for this fixed point was also located on the return map.

## 5.3    Results

All methods discussed above were applied to breathing waveforms recorded using Respiration Belt from Vernier Software and Technologies (Oregon, USA).  Flowchart showing the first section of LabView code is displayed in Figure 5-1. A snapshot of the LabView code is shown in (a) corresponding to the front panel shown in (b) used to acquire data. The sample rate (samples/ sec) and the length of data acquisition can be varied. Continuous baseline removal which accounts for drift in the data is also implemented here. The mutual information method and the recurrence plot constructed using Matlab code embedded into the Labview program is shown in (c) and (d) respectively. Finally once the user selects the appropriate UPO, the automatic peak detection program lists the number of peaks and its respective location as shown in (e). The respiratory signal from first peak to last peak (or trough to trough) is appended back to back to form a continuous guiding waveform. The front panel used for coaching and its corresponding Labview code(second section) is shown in (a) and (b) respectively. The volunteer can choose between a waveform or a moving bar as per convenience. Again, continuous baseline removal is performed to account for any drift.

### 5.3.1  Recurrence Quantification Analysis

A waveform was acquired from a sample volunteer used for training and after visual guidance. Recurrence quantification analysis was performed on both waveforms. The Recurrence Rate for both data was set to 1. Both breathing patterns had a delay time based on first minima of

mutual information method equal to 16, with the embedding dimension equal to 4. The RQA parameters $L_{avg}$, percent Determinism, Divergence, $L_{max}$, and Entropy is tabulated in Table 5-1. It can be seen that there is slight improvement in Determinism and Lavg, and significant improvement in Lmax.
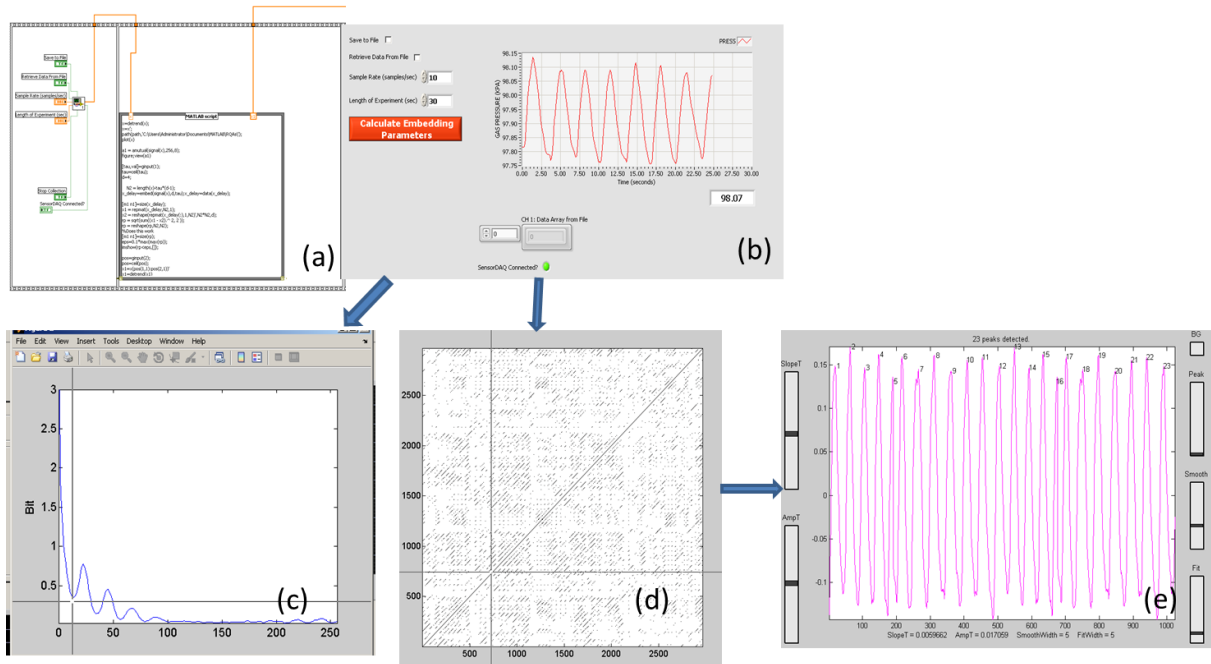


**Figure 5-1:** Flowchart showing the first section of Labview code is shown here. A snapshot of the LabView code is shown in (a) corresponding to the front panel shown in (b) used to acquire data. The sample rate (samples/ sec) and the length of data acquisition can be varied. The mutual information method and the recurrence plot constructed using Matlab code embedded into the Labview program is shown in (c) and (d) respectively. Finally once the user selects the appropriate UPO, the automatic peak detection program lists the number of peaks and its respective location as shown in (e).

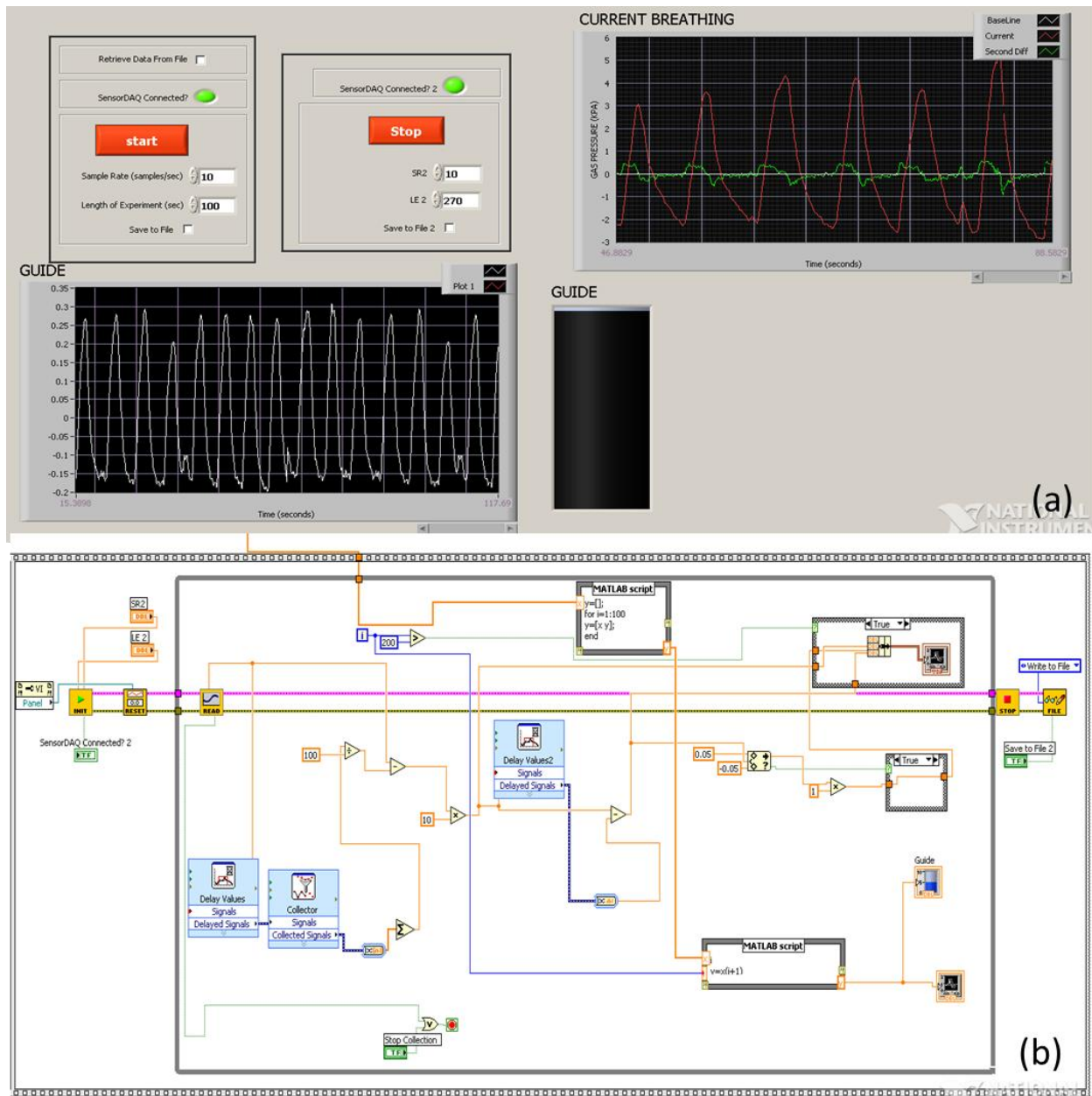**Figure 5-2:** The front panel used for coaching and its corresponding Labview code (second section) is shown in (a) and (b) respectively. The volunteer can choose between a waveform or a tank filling guide as per convenience.
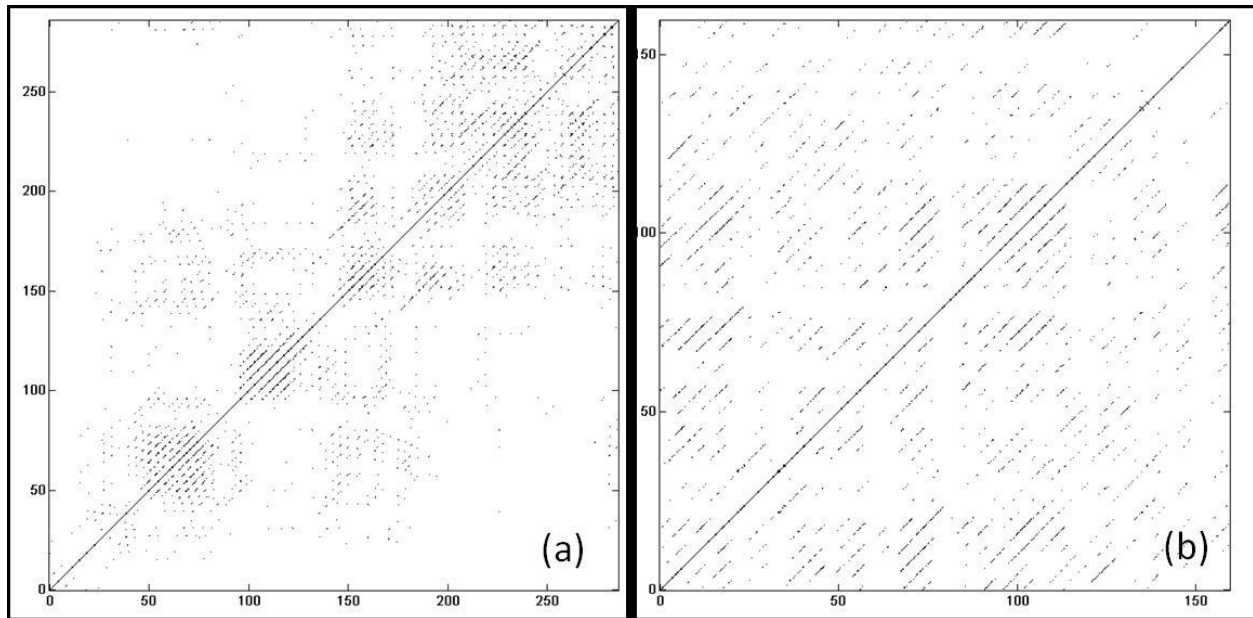
**Figure 5-3:** Recurrence plot of the training breathing signal is shown in (a) and the Recurrence plot for time series acquired after video guidance based on the volunteers UPO is displayed in (b). Visually, one can see longer diagonals in the coached breathing waveform.

The Recurrence plot of the breathing pattern used for training vs the breathing pattern obtained after guidance is shown in Figure 5-3(a) and 5-3(b) respectively.

|  | Recurrence Rate | % DET | $L_{avg}$ | $L_{max}$ | DIV | ENTR |
|---|---|---|---|---|---|---|
| Training Data | 1.0 | 0.7480 | 3.2915 | 39 | 0.0256 | 1.5455 |
| Guided Breathing Data | 1.0 | 0.8097 | 3.8676 | 59 | 0.0169 | 1.8065 |

**Table 5-1**: RQA Parameters for training breathing data and guided breathing data for the volunteer whose Recurrence Plots shown in Figure 5-3.

## 5.3.2 Control Algorithm

The breathing cycle of the initial 300 seconds was analyzed with the automatic peak detection algorithm. The return map of the IBP is shown in Figure 5-4 (points 20 through 27, 50

through 54). The UPO selected corresponds to the point z*, also point 21 shown in the figure. Based on the return map, from point 20 to 21, the system moves toward the unstable fixed point. This means that the point 20 must be close to the stable manifold (shown in red in Figure 5-4). Points 22 and 23 still lie in the vicinity of the fixed point before moving to point 24 (the far left point), followed by point 25( to the far right corner). Points 24 through 27 diverge from point 21 revealing an unstable manifold (shown in green in Figure 5-4).
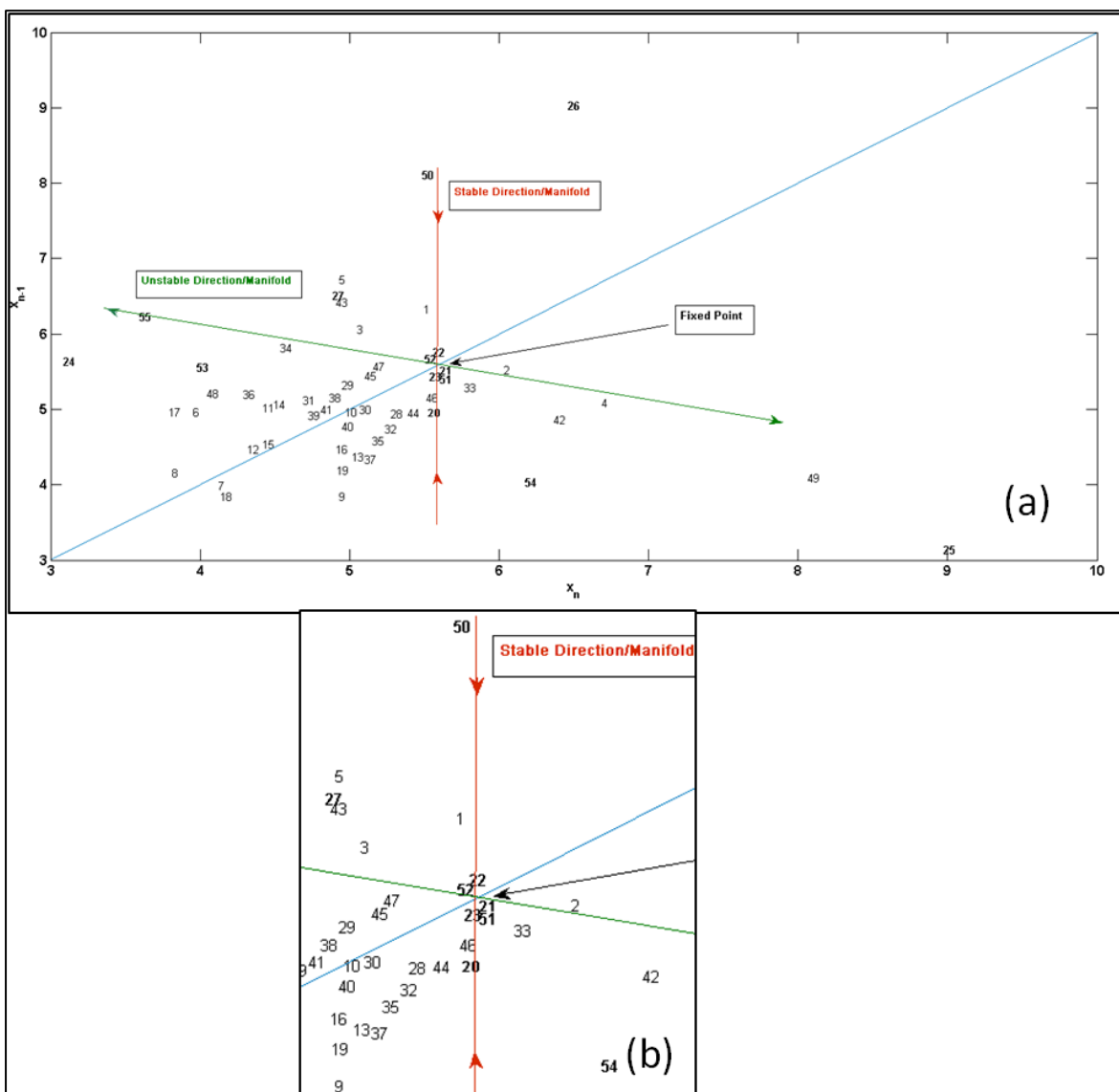
**Figure 5-4:** (a) Return Map of the training breathing waveform is shown in (a). The fixed point for Point 23 and points 22,23 in the vicinity of the fixed point is also shown. The red Line shows the stable manifold , and the green line represents the unstable manifold . The Return Map zoomed in around the fixed point is shown in (b). Refer to Section 3.2 for detailed explanation of the return map.

The volunteer returns to this stable manifold at point 50, and again coming under the influence of the stable manifold, gets to point 51 in the vicinity of z*(Point 21), and stays there for one more cycle(Point 52), before diverging again under the influence of the unstable manifold.

## 5.4   Discussion and Conclusion

We have summarized here, the theory behind Chaos Control and have established a method to pick an Unstable Periodic Orbit, in other words a fixed point in the return map which is used as a control set point. Coaching the patient with the UPO of his/her own breathing improves the reproducibility of breathing, based on the RQA parameters. We have also demonstrated how to construct a return map and pick a stable and unstable direction from a patients breathing pattern. However, studies on more patients multiple times will have to be done to establish if coaching one with the volunteers own UPO produces a desirable result. Locating stable and unstable manifold was quite straightforward on the return map for this volunteers breathing pattern. However, this might be challenging and needs ongoing effort towards realtime system for automatic detection of these manifolds. It is also of interest to note that strong stable and unstable manifolds could not be detected for the first UPO. It is also important to compare

different methods of coaching , such as simple audio instructions of "*Breathe in, Breathe out*" to see if some patients could benefit with a simple system of coaching.

The future work entails building a realtime system that can build and check the position of the breathing pattern based on IBP on a realtime basis for application of suitable perturbation. It would be of interest to check different modes of perturbation/feedback which could be visual, audio or sensory or a combination of the three.

## 5.5   Reference

Baker G L 1995 Control of the chaotic driven pendulum *American Journal of Physics* **63** 832-8

Garfinkel A, Spano M L, Ditto W L and Weiss J N 1992 Controlling cardiac chaos *Science* **257** 1230-5

Haasbeek C J A, Spoelstra F O B, Lagerwaard F J, van Sörnsen de Koste J R, Cuijpers J P, Slotman B J and Senan S 2008 Impact of audio-coaching on the position of lung tumors *International Journal of Radiation Oncology\* Biology\* Physics* **71** 1118-23

Keall P J, Mageras G S, Balter J M, Emery R S, Forster K M, Jiang S B, Kapatoes J M, Low D A, Murphy M J and Murray B R 2006 The management of respiratory motion in radiation oncology report of AAPM Task Group 76 *Med Phys* **33** 3874

Liu H H, Balter P, Tutt T, Choi B, Zhang J, Wang C, Chi M, Luo D, Pan T and Hunjan S 2007 Assessing respiration-induced tumor motion and internal target volume using four-dimensional computed tomography for radiotherapy of lung cancer *International Journal of Radiation Oncology\* Biology\* Physics* **68** 531-40

Mutaf Y, Antolak J and Brinkmann D 2007 The impact of temporal inaccuracies on 4DCT image quality *Med Phys* **34** 1615

Neicu T, Berbeco R, Wolfgang J and Jiang S B 2006 Synchronized moving aperture radiation therapy (SMART): improvement of breathing pattern reproducibility using respiratory coaching *Phys Med Biol* **51** 617

Ott E, Grebogi C and Yorke J A 1990 Controlling chaos *Physical review letters* **64** 1196-9

Persson G F, Nygaard D E, Olsen M, Juhler-Nøttrup T, Pedersen A N, Specht L and Korreman S S 2008 Can audio coached 4D CT emulate free breathing during the treatment course? *Acta Oncologica* **47** 1397-405

Scholl E and Schuster H G 2008 Handbook of chaos control. Wiley-VCH, Weinheim)

Senan S, De Ruysscher D, Giraud P, Mirimanoff R and Budach V 2004 Literature-based recommendations for treatment planning and execution in high-dose radiotherapy for lung cancer *Radiother Oncol* **71** 139-46

Shinbrot T, Ott E, Grebogi C and Yorke J A 1990 Using chaos to direct trajectories to targets *Physical review letters* **65** 3215-8

Slutzky M and Mogul D 2000 Modification of epileptiform bursting using chaos control. IEEE) pp 1425-8 vol. 2

Smale S 1966 DIFFERENTIABLE DYNAMICAL SYSTEMS1

Tewatia D K, Tolakanahalli R P, Paliwal B R and Tome W A 2011 Time series analyses of breathing patterns of lung cancer patients using nonlinear dynamical system theory *Phys Med Biol* **56** 2161-81

Tolakanahalli R, Tewatia DK, Tome WA 2012 Time series prediction of lung cancer patients' breathing pattern based on nonlinear dynamics *Phys Med Biol (submitted)*

van Sörnsen de Koste J R, Lagerwaard F J, Nijssen-Visser M R J, Graveland W J and Senan S 2003 Tumor location cannot predict the mobility of lung tumors: a 3D analysis of data generated from multiple CT scans *International Journal of Radiation Oncology* Biology* Physics* **56** 348-54

# Chapter 6. Conclusions and future work

Based on almost two decades of research and published peer reviewed work, it is well known that intensity modulated radiotherapy (IMRT) is a choice of treatment whenever a superior target dose conformity is required while limiting dose to critical organs within tolerance and sparing normal tissue as much as possible. However, the dose distribution from any type of an IMRT plan is susceptible to variation in the presence of intrafractional motion during the treatment delivery process. The work presented in this thesis is a foundation for building a realtime patient specific 4D treatment suite based on non-linear dynamics. This in combination with realtime 4D imaging and 4D tracking methodologies takes us a step further in making 4D treatments robust, accurate and available to those who can comply with the requirements of 4D treatments such as reproducibility and predictability of breathing. We have addressed many different challenges faced due to variation in respiratory dynamics and we demonstrate how it can be used for developing personalized input to a 4D IGRT treatment suite. Recognizing and establishing deterministic chaos in time series is an important step towards application of other nonlinear algorithms for prediction and control. The initial work presented here extends our prior work and uses surrogate methods to establish deterministic chaos. We show that the data series under consideration is not generated by i.i.d or linear Gaussian noise passed through a non-linear filter. Indeed for most patients, hypothesis that they are highly periodic and not chaotic is also rejected. This work opened the way for nonlinear analysis and validates the use of promising techniques for prediction and control which were explored in the subsequent chapters.

Robust implementation of any lung tumor motion management technique solely depends on goodness of breathing pattern prediction because of system latency issues. Exactness of results

obtained based on linear or nonlinear prediction methodologies are based how closely our used methodology is able untangle the actual dynamics of the given system. From the cohort of patients studied, we established that N-step ahead non-linear prediction methods yield better prediction results than an N-step ahead adaptive linear autoregressive prediction. Hence, we may consider that the use of non-linear prediction methods for prediction the breathing pattern of lung cancer patients may lead to improved, robust and accurate long-term prediction that can be used to account for system latencies. It has also been shown that a prediction engine based on nonlinear dynamics has a larger prediction horizon than other methods if an appropriate time delay and embedding dimension are chosen. With the advent of newer tumor tracking technologies such as the Calypso tracking system (Calypso, Seattle, Washington), RealEyeTM Motion (Navotek Medical Ltd, Yokneam, Israel), or real time MR Radiotherapy systems like the one being developed by Viewray (Viewray Inc., Cleveland, OH) with which it will be possible to acquire real-time MR images at a frame rate of 4 images/sec the presented nonlinear prediction methods can be directly implemented on the tumor motion coordinates. LAM which is computationally very inexpensive and whose performance is not sensitive to imaging frequency is more desirable for prediction of real-time tumor coordinates.

As established, only short term prediction is possible for chaotic signals due to its inherent sensitivity to initial conditions. However, a much larger prediction horizon can be achieved if patients can be guided to follow a regular and reproducible breathing pattern.

Before this can be achieved, it is important to be able to identify patients who will be amenable to coaching and prediction and thus benefit from the 4D treatment strategies, and classify those who will have better tumor control with ITV based treatments. It is also important to identify the patients who will benefit by coaching for longer prediction horizons. We thus

extended the work and used a quantitative analysis tool that can be used as a guide for selection of appropriate 4D treatment strategy for lung cancer patients. In Recurrence Quantification Analysis , described in Chapter 4, we show that RQA can be used as a good assessment for predictability and complexity of the patient's breathing pattern. $K_2$ values calculated are invariant quantities and give an approximation of how chaotic the signal under consideration is. We have also shown the use of Time Resolved RQAs for automatic detection of UPOs that can be used for coaching patients. The future work in RQAs includes assessment of patient breathing patterns including non-stationary signals that can introduce huge prediction errors. Quantitative Recurrence Analysis can be a very powerful mathematical tool that can be used for segregating patients into different 4D treatment strategies, based on their variability of breathing.

This brings us to the last part of the thesis where we have summarized the theory behind Chaos Control and have established a method to pick an Unstable Periodic Orbit, in other words a fixed point in the return map which can be used as a control set point. We have demonstrated that coaching the patient with the UPO of an individual's own breathing may improve the reproducibility of breathing, based on the RQA parameters. We have also demonstrated how to construct a return map and pick a stable and unstable direction from a patients breathing pattern. Automatic localization of stable and unstable manifold might be challenging and needs ongoing effort towards building a realtime system. The future work entails building a realtime system that can build and check the position of the breathing pattern on a realtime basis for application of suitable perturbation. It would be of interest to check different modes of perturbation/feedback which could be visual, audio or sensory or a combination of the three.

With the advent of newer tumor tracking technologies such as the Calypso tracking system (Calypso, Seattle, Washington), RealEyeTM Motion (Navotek Medical Ltd, Yokneam, Israel), or

real time MR Radiotherapy systems like the one being developed by Viewray (Viewray Inc., Cleveland, OH) with which it will be possible to acquire real-time MR images at a frame rate of 4 images/sec coupled with fast treatment like VMAT technologies, tumor tracking can be a reality. The tools described in this thesis can be used in conjunction with 4D treatment methodologies, such as CyberKnife, BSD for a complete motion management suite.